Met.O.890

METEOROLOGICAL OFFICE

Scientific Paper No. 34

The Meteorological Office Operational 10-level Numerical Weather Prediction Model (December 1975)

by D. M. BURRIDGE, Ph.D. and A. J. GADD, Ph.D.

LONDON: HER MAJESTY'S STATIONERY OFFICE

£1.25 NET

Met.O.890

METEOROLOGICAL OFFICE

Scientific Paper No. 34

The Meteorological Office Operational 10-level Numerical Weather Prediction Model (December 1975)

by D. M. BURRIDGE, Ph.D. and A. J. GADD, Ph.D.

LONDON

HER MAJESTY'S STATIONERY OFFICE

U.D.C. 551.509.313

© *Crown copyright 1977*

ISBN 0 11 400300 9

Contents

Notation v

Physical constants vii

Grid and geographical constants vii

Summary 1

1. Introduction 1

2. System of equations 3

3. The Lax-Wendroff integration scheme 4

4. The split semi-implicit integration scheme 11

5. Lateral boundary conditions 20

6. Precipitation processes 21

7. Surface exchanges 25

8. Convective adjustments 33

Bibliography 38

NOTATION

a	horizontal grid length on the polar stereographic map projection
$A_{k+½}$	a set of constants used to convert 100-mb layer thicknesses to potential temperatures (see Table X on p.38)
b	γ_c/γ_d
$B_{k+½}$	a set of constants used to convert 100-mb layer thicknesses to temperatures (see Table X)
C_H, C_M, C_L	fractional cover of high, medium, low cloud
c_i	conduction coefficient used at sea ice surfaces
c_p	specific heat of air at constant pressure
C_D, C_E	drag coefficient, exchange coefficient for sensible and latent heat
C_k	$h'_{k+½}/h'_{k-½}$ when the static stability is neutral for convection
$E_{k+½}$	evaporation constants for rain and snow (see Tables III and IV)
f	Coriolis parameter
F', F	transmission function for clear, cloudy atmosphere
F_G	flux of heat into ground
F_H, F_W	flux of heat, water vapour into atmosphere at 1000 mb
g	acceleration due to gravity
h	height of an isobaric surface
$h'_{k+½}$	thickness of 100-mb layers
H	height of topography
$\mathbf{k}$	unit vertical vector
K	lateral diffusion coefficient
L, L_f, L_s	latent heat of condensation, fusion, sublimation
L'_o, L_o	net upward long-wave radiation at the ground for clear, cloudy skies
M_k	liquid water falling through level k in a time-step
m	map magnification factor
p	pressure
P_k	rate of rainfall at level k
q	$\frac{L}{c_p}\left(\frac{\partial r_s}{\partial T}\right)_p$
Q	rate of diabatic heating due to precipitation, surface exchanges, convective adjustments
r	humidity mixing ratio
r_s	saturation humidity mixing ratio
R	gas constant
R_N	net radiation flux at ground
S	solar constant
T	temperature
t	time
u, v	horizontal velocity components
u^*, v^*	u/m, v/m
$\mathbf{V}$	horizontal velocity vector
w	Dz/Dt
W	rate of change of humidity mixing ratio due to precipitation, surface exchanges, convective adjustments

X	relative humidity (expressed as a decimal fraction)
x, y	co-ordinates on the polar stereographic map projection
z	height
α	albedo
β	static stability parameter
γ	$-\partial T/\partial z$
$\gamma_c, \gamma_d, \gamma_s$	neutral, dry adiabatic, saturated adiabatic values of γ
δ	solar declination
$\delta_x, \delta_y, \delta_p$	finite difference operators
δt	time-step of integration
Δp	vertical grid length, i.e. 100 mb
ϵ	ratio of molecular weights of water and dry air
θ	potential temperature
κ	R/c_p
λ	longitude
μ	m^2
ν	evaporation constant
ρ	density
τ	frictional stress
τ^*	τ/m
ϕ	latitude
χ	F_G/R_N
ψ	solar angle
ω	Dp/Dt

SUFFIXES

x, y, p, t	partial differentiation
i, j	horizontal grid-point indices
k	pressure-level index (k=1 at 100 mb, k=10 at 1000 mb)
$k+\frac{1}{2}$	layer index for layer between pressure level k and pressure level $k+1$
o	indicates a value at the ground
a	indicates a value at the 10-metre level
s	indicates a value at the sea/ice interface

PHYSICAL CONSTANTS

c_p	1004.64	J kg^{-1} K^{-1}
R	287.04	J kg^{-1} K^{-1}
c_p/R	3.5	
$\kappa = R/c_p$	0.285 714 3	
g	9.8	m s^{-2}
g/R	$3.414\ 158 \times 10^{-2}$	K m^{-1}
$\gamma_d = g/c_p$	$9.754\ 738 \times 10^{-3}$	K m^{-1}
L	2.500×10^6	J kg^{-1}
L_f	0.334×10^6	J kg^{-1}
L_s	2.834×10^6	J kg^{-1}
ϵ	0.622	
ρ_{10}	1.212	kg m^{-3}

GRID AND GEOGRAPHICAL CONSTANTS

The x, y grid is drawn on a polar stereographic map projection with the origin at the north pole and with the x-axis pointing along longitude 55°E.

For the octagon $a = 3.266\ 836\ 35 \times 10^5$ m and the co-ordinates of the corners of the grid are $(\pm 12a, \pm 30a)$ and $(\pm 30a, \pm 12a)$.

For the rectangle $a = 1.088\ 945\ 45 \times 10^5$ m and the co-ordinates of the corners of the grid are $(-18a, -14a)$, $(45a, -14a)$, $(45a, -61a)$, $(-18a, -61a)$.

Latitude ϕ and longitude λ are related to x and y by

$$\phi = \sin^{-1}\left[\frac{4R_E^2 - x^2 - y^2}{4R_E^2 + x^2 + y^2}\right] \qquad \lambda = \lambda_0 + \tan^{-1}\left(\frac{y}{x}\right)$$

where R_E (radius of the earth) = $6.367\ 3 \times 10^6$ m and λ_0 corresponds to 55°E.

The map factor m and Coriolis parameter f are defined as functions of latitude by

$$m = \frac{2}{1 + \sin\phi} \qquad f = 2\Omega \sin\phi$$

where $\Omega = (2\pi/86\ 400)$ s^{-1} and $\pi = 3.141\ 59$.

The Meteorological Office Operational 10-level Numerical Weather Prediction Model (December 1975)

by D. M. Burridge, Ph.D. and A. J. Gadd, Ph.D.

SUMMARY

A full description is given of the 10-level numerical model of the atmosphere which is used operationally each day in the Meteorological Office to provide guidance for short- and medium-range forecasts. The present paper may in many respects be seen as a sequel to *Scientific Paper* No. 32, but it is complete in itself and describes the state of the model in December 1975. The paper makes reference both to the limited-area fine-mesh version of the model (the development of this version up to the end of 1969 was described in *Scientific Paper* No. 32) and to the coarse-mesh version which provides forecasts for most of the northern hemisphere. The paper deals in turn with the basic system of equations used in the model, with the two finite-difference integration schemes which have been used to compute forecasts, with lateral boundary conditions, and finally with the physical and sub-grid-scale processes which are represented in the model.

1. INTRODUCTION

This paper describes the 10-level primitive-equation model of the atmosphere which has formed the basis of operational numerical weather prediction in the Meteorological Office since August 1972. The model now has a history of about 10 years and was first described by Bushby and Timpson (1967). The model has been subject to a continuous process of development; Benwell *et alii* (1971) gave a full description of the state of development at the end of 1969. The present paper describes the model as it was used operationally in December 1975 but is in no sense a final statement, since research is currently in progress on several aspects of the model.

Whilst the scope of this paper is confined to the forecast model itself, it should be remembered that the operational forecasting system includes many other computations which have an important bearing on the quality of information supplied to users. These other computations are concerned with data extraction, objective analysis, initialization, tropopause and maximum-wind modelling, output in various media, verification and so on. The entire sequence is repeated on a 12-hour cycle.

The 10-level model is used to compute forecasts in the following two domains, which are illustrated in Figure 1.

(a) A domain defined by an octagonal grid of 3037 points on a polar stereographic map projection. The grid circumscribes latitude 15°N and the grid spacing is 300 km at 60°N. Forecasts for three days ahead are computed twice daily; once a day a forecast is extended to six days.

(b) A domain defined by a 64 x 48 rectangular grid on a polar stereographic map projection. This domain includes western Europe and the North Atlantic Ocean and the grid spacing is 100 km at 60°N. Forecasts for one-and-a-half days ahead are computed twice daily.

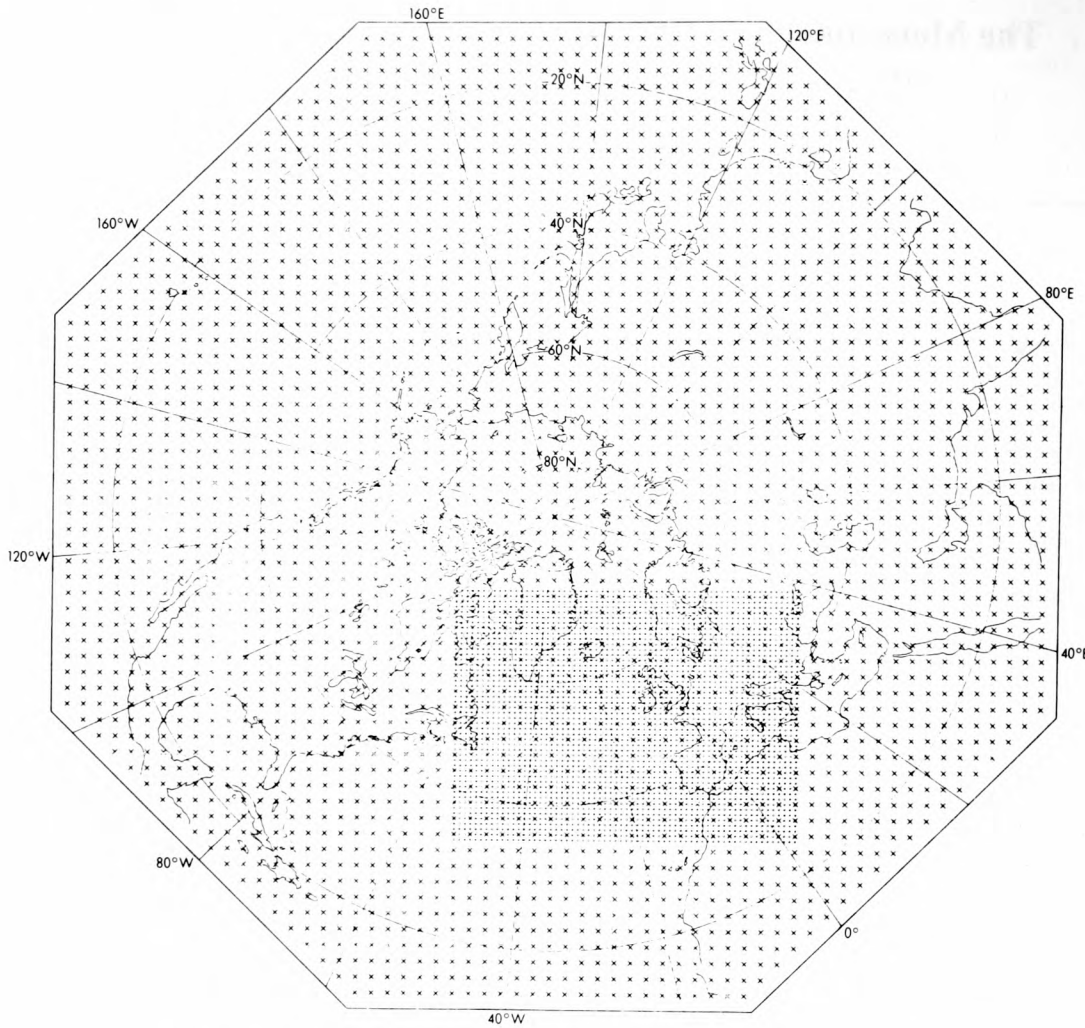

FIGURE 1. Rectangle and octagon forecast area grid points

The system of equations used in the model is set out in section 2. Two integration schemes have been used to integrate the equations, and these are described separately in sections 3 and 4. The first is a Lax-Wendroff scheme which is no longer used operationally but a description of which is included for completeness. The second is a split semi-implicit integration scheme due to Burridge (1975) which offers substantial economies in computing time over the Lax-Wendroff scheme. The forecasts are currently computed using 15-minute time-steps for the octagon and 12-minute steps for the rectangle.

Lateral boundary conditions are described in section 5. In the octagon forecasts the boundary values remain constant in time, whilst for rectangle forecasts time-dependent boundary conditions are derived from octagon forecasts.

Physical processes represented in the model at present are precipitation (section 6), surface exchange (section 7), and small-scale convection (section 8).

Pressure is used as the vertical co-ordinate. The atmosphere is modelled by a layer of air extending from 100 mb to 1000 mb, at which level a topographically dependent boundary condition is applied. The 10 co-ordinate surfaces are spaced at intervals of 100 mb. Horizontal velocity components (u and v), the thicknesses of the 100-mb layers (h'), and the height of the 1000-mb surface (h_{10}) are calculated from predictive equations, whilst the vertical velocity and the heights of the other co-ordinate surfaces are determined diagnostically. Humidity mixing ratio (r) is predicted in the seven lowest layers, whilst the upper two layers are assumed to be dry.

2. SYSTEM OF EQUATIONS

2.1. *Introduction*

Horizontal Cartesian co-ordinates (x, y) on a polar stereographic map projection and pressure (p) form the spatial co-ordinate system. The map magnification factor (m) is defined by $m = 2/(1 + \sin\phi)$, where ϕ is latitude, and is the ratio of an infinitesimal distance on the map projection to the corresponding distance on the earth's surface. The velocity components (u, v, ω) are defined by

$$u = \frac{1}{m}\frac{\mathrm{D}x}{\mathrm{D}t}, \quad v = \frac{1}{m}\frac{\mathrm{D}y}{\mathrm{D}t}, \quad \omega = \frac{\mathrm{D}p}{\mathrm{D}t}.$$

The horizontal vector $\mathbf{v}$ is defined by (u, v) and the vector operators ∇ and div are correspondingly used in a two-dimensional, horizontal sense. Derivatives with respect to pressure (p) and time (t) are indicated by suffixes; k is a unit vertical vector.

In order to account fully for the curvilinear co-ordinate system on a stereographic plane it is convenient to define

$$\mathbf{v}^* = \mathbf{v}/m, \quad \tau^* = \tau/m, \quad \text{and} \quad \mu = m^2,$$

where τ is the frictional stress.

2.2. *Prognostic equations*

(a) *momentum equation*

$$\mathbf{v}^*_t + \mu\,(\mathbf{v}^*\cdot\nabla)\mathbf{v}^* + \omega\mathbf{v}^*_{\mathrm{p}} + f\mathbf{k}\wedge\mathbf{v}^* + g\nabla h + \tfrac{1}{2}|\mathbf{v}^*|^2\nabla\mu = -g\tau^*_{\mathrm{p}} \qquad \ldots (2.1)$$

(b) *thermodynamic equation*

$$h_{\mathrm{pt}} + \mu\mathbf{v}^*\cdot\nabla h_{\mathrm{p}} + \omega\left[h_{\mathrm{pp}} + \frac{(1-\kappa)h_{\mathrm{p}}}{p}\right] = -\frac{\kappa Q}{gp} \qquad \ldots (2.2)$$

(c) *humidity equation*

$$r_{\mathrm{t}} + \mu\mathbf{v}^*\cdot\nabla r + \omega r_{\mathrm{p}} = W. \qquad \ldots (2.3)$$

Q and W represent the effects of precipitation, surface exchanges, and small-scale convection. A further prognostic equation, the 1000-mb-height tendency equation (2.7), is

obtained from the lower boundary condition (see below). The prognostic equations also include a linear horizontal-diffusion term; this is regarded as a filtering device and is described in sections 3 and 4.

2.3. *Diagnostic equations*

The single diagnostic relationship which is explicitly required is the continuity equation

$$\omega_p + \mu \operatorname{div} \mathbf{v}^* = 0. \qquad \ldots (2.4)$$

The hydrostatic equation

$$h_p + \frac{RT}{gp} = 0 \qquad \ldots (2.5)$$

is implicit in the derivation of the thermodynamic equation (2.2) and is also used to obtain temperature (T) or potential temperature (θ) when required. The vertical velocity ω and height h are calculated by vertical integration of ω_p and h_p using the boundary conditions set out below.

2.4. *Boundary conditions*

(a) at $p = 50$ mb $\qquad \omega = 0 \qquad \ldots (2.6)$

(b) at $p = 1000$ mb $\qquad h_t + \mu \mathbf{v}^* \cdot \nabla h + \omega h_p = \mu \mathbf{v}^* \cdot \nabla H. \qquad \ldots (2.7)$

In this lower boundary condition H is the topography height and the condition corresponds to $w \equiv Dh/Dt = \mathbf{v} \cdot \nabla H$ at 1000 mb. For lateral boundary conditions, see section 5.

3. THE LAX-WENDROFF INTEGRATION SCHEME

3.1. *Introduction*

In this section a description is given of the explicit integration scheme (essentially similar to that originally used by Bushby and Timpson (1967)) which was used (until March 1973 in the case of the rectangle and until October 1974 in the case of the octagon) to integrate the equations of section 2. The integration scheme is based on a two-step Lax-Wendroff method which is applied to the system of equations with τ, Q, and W set to zero. The effects represented by these terms are accounted for separately.

Lax-Wendroff integration schemes are based on the calculation of the value (Z_{n+1}) of a variable Z at time $(n+1)\,\delta t$ from its value (Z_n) and first two time-derivatives ($\dot{Z}_n$, $\ddot{Z}_n$) at time $n\,\delta t$ using a truncated Taylor series.

$$Z_{n+1} = Z_n + \delta t \dot{Z}_n + \tfrac{1}{2}\,\delta t^2\, \ddot{Z}_n. \qquad \ldots (3.1)$$

In simple cases $\dot{Z}_n$ and $\ddot{Z}_n$ may be calculated directly by using the differential equations, but the complexity of the system of equations set out in section 2 demands that the following two-step approximation to equation (3.1) be used.

$$Z_{n+½} = Z_n + ½\,\delta t\,\dot{Z}_n \qquad \ldots (3.2)$$

$$Z_{n+1} = Z_n + \delta t\,\dot{Z}_{n+½} \,. \qquad \ldots (3.3)$$

Equation (3.2) represents a forward time-step over half the time-step of integration; equation (3.3) represents a centred step over the full time-step δt. The complete integration scheme described by equations (3.2) and (3.3) is accurate to the second order in time. Algorithms are required for the calculation of $\dot{Z}_n$ and $\dot{Z}_{n+½}$ and these are obtained through finite-difference approximations as described below.

3.2. *Finite-difference grid*

The two-step Lax-Wendroff scheme is used in conjunction with the Eliassen grid which is staggered in space and time as illustrated in Figure 2. Notice that h, h_p and r are all calculated at the basic grid points of the mesh (the points shown in Figure 1), whilst u, v and ω are calculated at points which are staggered with respect to the basic grid points. The variables all change their positions at the intermediate stages $(n+½)\,\delta t$. A staggering in space and time of this kind is an essential feature of a proper application of Lax-Wendroff techniques. Widely held misconceptions have arisen about the performance of Lax-Wendroff schemes from considerations of their properties when applied to unstaggered grids.

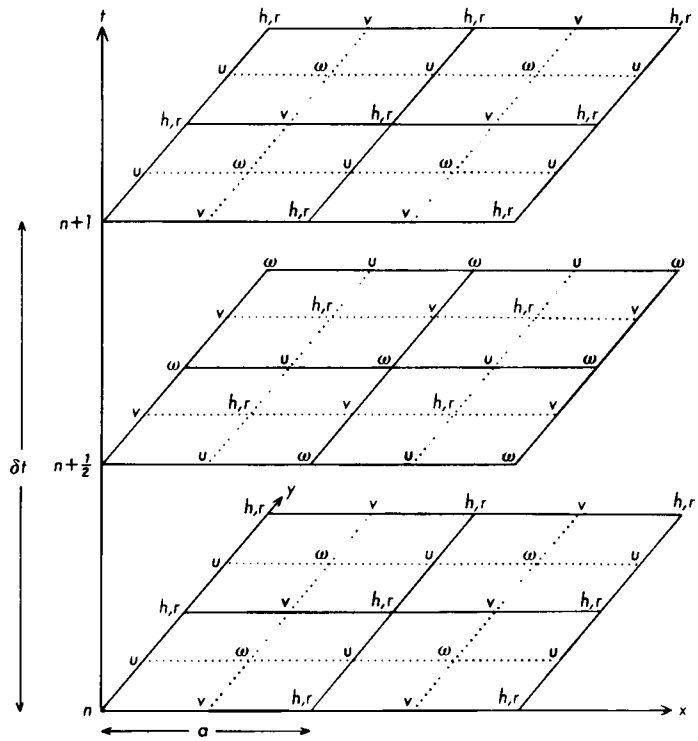

FIGURE 2. An x-y-t diagram illustrating the space and time staggering of the Eliassen grid, used in conjunction with the Lax-Wendroff integration scheme

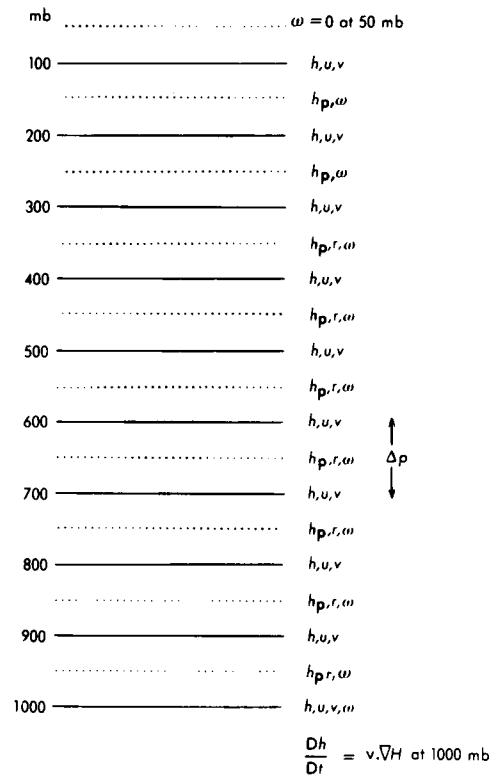

FIGURE 3. The vertical deployment of variables in the 10-level model

The vertical deployment of variables in the 10-level model is illustrated in Figure 3. Notice that u, v and h are calculated at the 10 isobaric co-ordinate surfaces, whilst h_p, r and ω are calculated at intermediate levels; ω is also calculated at 1000 mb. (The positioning of the ωs differs from that originally adopted in the 10-level model. The change was made in December 1972 in order to achieve a more desirable vertical structure of the high-order gravity-wave modes.)

The following finite difference for h_p is used

$$(h_p)_{k+\frac{1}{2}} = \frac{h_{k+1} - h_k}{\Delta p} = \frac{-h'_{k+\frac{1}{2}}}{\Delta p}. \qquad \ldots (3.4)$$

where h' is the thickness of a 100-mb layer, and $\Delta p = 100$ mb. Thicknesses of the 100-mb layers may be used as the thermodynamic variable by substituting equation (3.4) into equation (2.2).

$$h'_t + \mu \mathbf{v}^* \cdot \nabla h' + \omega\beta = \frac{\kappa Q \Delta p}{gp}. \qquad \ldots (3.5)$$

In this equation $\beta = -\Delta p \left(h_{pp} + \frac{(1-\kappa)h_p}{p}\right)$ is a measure of the static stability; the calculation of β is discussed below.

3.3. *Finite-difference approximations*

The following notation is used in describing finite-difference approximations, with similar conventions for y and p derivatives and averages.

$$(\delta_x Z)_i = \frac{1}{a}\,(Z_{i+\frac{1}{2}} - Z_{i-\frac{1}{2}})$$

$$(\overline{Z}^x)_i = \tfrac{1}{2}(Z_{i+\frac{1}{2}} + Z_{i-\frac{1}{2}})$$

Here a is the grid length on the polar stereographic map projection.

With τ, Q, and W set to zero, the following finite-difference approximations to the prognostic equations (2.1), (3.5), (2.3), and (2.7) are used.

$$\dot{u}^* = -\mu[\overline{u^*}^{xy}\delta_x\overline{u^*}^{y} + v^*\delta_y\overline{u^*}^{x}] - \overline{\omega}^{yp}\overline{\delta_p\overline{u^*}^{xy}}^{p} - \tfrac{1}{2}[(\overline{u^*}^{xy})^2 + (\overline{v^*})^2]\delta_x\mu + fv^* - g\delta_x h \quad \ldots (3.6)$$

$$\dot{v}^* = -\mu[u^*\delta_x\overline{v^*}^{y} + \overline{v^*}^{xy}\delta_y\overline{v^*}^{x}] - \overline{\omega}^{xp}\overline{\delta_p\overline{v^*}^{xy}}^{p} - \tfrac{1}{2}[(u^*)^2 + (\overline{v^*}^{xy})^2]\delta_y\mu - fu^* - g\delta_y h \quad \ldots (3.7)$$

$$\dot{h}' = -\mu[\overline{u^*}^{xp}\delta_x\overline{h'}^{y} + \overline{v^*}^{yp}\delta_y\overline{h'}^{x}] \quad \omega\overline{\beta}^{xy} \quad \ldots (3.8)$$

$$\dot{r} = -\mu[\overline{u^*}^{xp}\delta_x\overline{r}^{y} + \overline{v^*}^{yp}\delta_y\overline{r}^{x}] - \omega\overline{\delta_p\overline{r}^{xy}}^{p} \quad \ldots (3.9)$$

$$\dot{h}_{10} = -\mu[\overline{u^*_{10}}^{x}\delta_x\overline{(h_{10} - H)}^{y} + \overline{v^*_{10}}^{y}\delta_y\overline{(h_{10} - H)}^{x}] + \frac{\omega_{10}\overline{h'}^{xy}_{9\cdot5}}{\Delta p} \quad \ldots (3.10)$$

These approximations may be used in both steps of the Lax-Wendroff scheme, given the deployment of variables illustrated in Figures 2 and 3. Since the topography height is stored only at the basic grid points of the mesh, $\overline{H}^{xy}$ replaces H in the second step in equation (3.10). Special measures are required near upper and lower boundaries. One-sided differences are used to estimate vertical derivatives at 100 mb and 1000 mb in equations (3.6) and (3.7) and at 350 mb and 950 mb in equation (3.9). $\overline{\omega}^{yp}$ is replaced by $\overline{\omega}^{y}$ at 1000 mb in equations (3.6) and (3.7).

Equation (2.4) is integrated by the following scheme to obtain ω when required.

$$\omega_{0\cdot5} = 0$$

$$\omega_{k+\frac{1}{2}} = \omega_{k-\frac{1}{2}} - \Delta p\mu(\delta_x u^*_k + \delta_y v^*_k)$$

$$\omega_{10} = \omega_{9\cdot5} - \tfrac{1}{2}\Delta p\mu(\delta_x u^*_{10} + \delta_y v^*_{10}),$$

where $k = 1,2, \ldots 9$. The heights h_k ($k = 1,2, \ldots 9$) are obtained by summation of h_{10} and the thicknesses $h'_{k+\frac{1}{2}}$ when required.

$$h_k = h_{k+1} + h'_{k+\frac{1}{2}},$$

where $k = 9,8, \ldots 1$.

3.4. *The integration cycle*

The first step of the Lax-Wendroff scheme is calculated as

$$Z_{n+½} = \bar{Z}_n^{xy} + ½\delta t \dot{Z}_n, \quad \ldots (3.11)$$

where $Z = (u^*, v^*, h', r, h_{10})$ in turn and the $\dot{Z}_n$ are calculated by using equations (3.6)–(3.10). $\omega_{n+½}$ and $h_{n+½}$ may then be diagnosed, and the second step of the scheme is similarly represented by

$$Z_{n+1} = Z_n + \delta t \dot{Z}_{n+½}. \quad \ldots (3.12)$$

The effects of the frictional stress τ and of horizontal filtering are included as described below before ω_{n+1} is calculated. Finally the effects represented by Q and W are added to h'_{n+1} and r_{n+1} as described in sections 6, 7 and 8.

3.5. *Fourth-order differences*

The finite-difference approximations used in equations (3.6)–(3.10) are such that the complete integration cycle represented by equations (3.11) and (3.12) is accurate to the second order in space and time. The general use of fourth-order accurate approximations to spatial derivatives would impose unacceptable computational penalties in terms of a reduced time-step for computational stability. However, it is possible to introduce fourth-order accuracy to certain terms without serious overheads, and with considerable theoretical improvements in advective phase speeds.

The finite-difference approximations used in the second step of the Lax-Wendroff integration scheme are modified in horizontal advection terms only by replacing the finite difference $(\delta_x Z)_i$ with

$$\frac{3}{2}\left(\frac{Z_{i+½} - Z_{i-½}}{a}\right) - \frac{1}{2}\left(\frac{Z_{i+3/2} - Z_{i-3/2}}{3a}\right)$$

and similarly for $\delta_y Z$. It may be shown that these modified finite-difference equations lead to a fourth-order accurate estimate of first derivatives arising from horizontal advection terms. The second derivatives which also arise from the horizontal advection terms continue to be estimated to second-order accuracy. (Further information on the fourth-order scheme is given by Gadd (1974); the scheme was used operationally from September 1972 onwards.)

3.6. *The static stability term*

The static stability term β in equation (3.5) is calculated by applying vertical finite differences to potential temperatures $\theta_{k+½}$ derived from the 100-mb layer thickness $h'_{k+½}$. Using equations (2.5) and (3.4) we have that

$$\theta_{k+½} = \left(\frac{p_{10}}{p_{k+½}}\right)^{\kappa} \frac{g p_{k+½}}{R} \frac{h'_{k+½}}{\Delta p} = A_{k+½}\ h'_{k+½} \text{ say.}$$

Centred difference approximations to $\partial\theta/\partial p$ are used except at 950 mb, where a one-sided difference is used, and at 150 mb, where an isothermal assumption is invoked. The following expressions for β are thus obtained.

$$\beta_{1\cdot5} = -\frac{\kappa\theta_{1\cdot5}}{A_{1\cdot5}p_{1\cdot5}}$$

$$\beta_{k+\frac{1}{2}} = \frac{1}{A_{k+\frac{1}{2}}}\left(\frac{\theta_{k+3/2} - \theta_{k-\frac{1}{2}}}{2\Delta p}\right),$$

where $k = 2,3, \ldots 8$.

$$\beta_{9\cdot5} = \frac{1}{A_{9\cdot5}}\left(\frac{\theta_{9\cdot5} - \theta_{8\cdot5}}{\Delta p}\right).$$

The method of calculating β described here is superior to the direct finite-difference approximation to

$$\beta = -\Delta p\,(h_{pp} + \frac{(1-\kappa)h_p}{p})$$

which was originally used in the 10-level model. (Further details are given by Gadd (1973); the method described above was used operationally from September 1973 onwards.)

3.7. *The friction terms*

Section 8.1 describes the calculation of the frictional tendencies $\dot{u}^*_F$ and $\dot{v}^*_F$. (Other variables are not directly affected by friction.) The friction terms are integrated by a forward step over the full time-step δt, since experience showed that computational instability could arise if these terms were included in the two-step Lax-Wendroff scheme. Hence equation (3.12) is modified to read

$$Z_{n+1} = Z_n + \delta t \dot{Z}_{n+\frac{1}{2}} + \delta t\,(\dot{Z}_F)_n. \qquad \ldots (3.13)$$

3.8. *Filtering*

Horizontal filtering is achieved where necessary by means of linear-diffusion terms added to the prognostic equations (2.1), (2.3), (2.7), and (3.5). The tendency due to the diffusion term and its finite-difference approximation are as follows.

$$\dot{Z}_D = K\nabla^2 Z = K\,(\delta_x\delta_x Z + \delta_y\delta_y Z).$$

The following values of the diffusion coefficient have been chosen in the light of experience. The units of K are $m^2 s^{-1}$.

(a) octagon

$$K = \begin{cases} 2 \times 10^5 + 250H & \text{north of } 21°\text{N, where } H \text{ is the topography height in metres.} \\ 3 \times 10^6 & \text{south of } 21°\text{N, i.e. in boundary zone.} \end{cases}$$

(b) rectangle

$$K = \begin{cases} 10^5 + 250H & \text{except in boundary zone.} \\ 10^6 & \text{within three grid lengths of the lateral boundary.} \end{cases}$$

The diffusion terms are included by a forward time-step, so that equation (3.13) is further modified as follows:

$$Z_{n+1} = Z_n + \delta t \dot{Z}_{n+\frac{1}{2}} + \delta t (\dot{Z}_F)_n + \delta t (\dot{Z}_D)_n. \quad \ldots (3.14)$$

3.9. *Special measures near lateral boundaries*

The lateral boundary conditions for the model are described in section 5. The height, humidity mixing ratio, and normal velocity component are specified at the boundary, and an enhanced diffusion coefficient is used in a narrow boundary zone (see section 3.8 above). For the Lax-Wendroff scheme the following additional measures are adopted at lateral boundaries.

(a) In the octagon model u and v velocity components are held constant within a half-grid-length distance from the lateral boundary. Additionally, where the boundary passes diagonally through the grid, u and v velocity components immediately outside the boundary are set equal to the average of the two nearest values inside the boundary, whilst ω is set to zero on the boundary. (These values are required for the first step of the Lax-Wendroff scheme.) Heights and humidity mixing ratios are interpolated along such diagonal boundaries to provide values needed in the second step of the integration scheme.

(b) In the rectangle model tangential velocity components are calculated on the boundary in the first step of the integration scheme by assuming that the normal gradient of the tangential velocity is zero at the boundary and also that ω is zero on the boundary.

3.10. *Criterion for computational stability*

It is not feasible to derive a criterion for computational stability for the application of the integration scheme to the complete non-linear equations set out in section 2. Experience has shown, however, that the stability criterion for the application of the scheme to a linearized form of the equations gives very reliable guidance on the choice of a time-step for the non-linear model itself.

The linearized set of equations is obtained by considering small perturbations of a uniform flow (U, V) in an atmosphere with some given vertical thermal structure (the ICAO standard atmosphere for example). Following Burridge (1975), the linearized equations applied at the 10 levels of the model may be decoupled into 10 sets of equations of the form

$$\left.\begin{aligned}
\frac{\partial a_k}{\partial t} &= -mU\frac{\partial a_k}{\partial x} - mV\frac{\partial a_k}{\partial y} + fb_k - mg\frac{\partial y_k}{\partial x} \\
\frac{\partial b_k}{\partial t} &= -mU\frac{\partial b_k}{\partial x} - mV\frac{\partial b_k}{\partial y} - fa_k - mg\frac{\partial y_k}{\partial y} \\
\frac{\partial y_k}{\partial t} &= -mU\frac{\partial y_k}{\partial x} - mV\frac{\partial y_k}{\partial y} - \frac{mc_k^2}{g}\left(\frac{\partial a_k}{\partial x} + \frac{\partial b_k}{\partial y}\right)
\end{aligned}\right\}, \quad \ldots (3.15)$$

where $k = 1,2, \ldots, 10$, and where the perturbation velocity components and heights are linear combinations of the new variables a_k, b_k, and y_k respectively, and the c_k are eigenvalues of a matrix defined by the vertical structure of the unperturbed atmosphere and the vertical finite differences of the integration scheme. Terms arising from variations in m, along with topographic, friction, diabatic heating and filtering terms, have been neglected in obtaining the above equations.

Following Farr and Lewis (1971) it may be shown that if the Lax-Wendroff scheme is applied to the above equations the following criterion must be satisfied for computational stability.

$$\delta t \leqslant \frac{a}{m\sqrt{2}\sqrt{(c_k{}^2 + U^2 + V^2)}}. \qquad \ldots (3.16)$$

Clearly the permissible time-step is set by the largest c_k, which Burridge (1975) calculated as 298 m s^{-1} for the ICAO atmosphere. This may be identified with the phase speed of the external gravity wave. In choosing time-steps for the 10-level model values of $\sqrt{(U^2 + V^2)}$ up to 100 m s^{-1} have been allowed for in the rectangle and values up to 150 m s^{-1} in the octagon.

4. THE SPLIT SEMI-IMPLICIT INTEGRATION SCHEME

4.1. *Introduction*

In this section we describe the semi-implicit integration scheme that is currently being used to integrate the equations of section 2; a detailed account of this method is given by Burridge (1975). The explicit Lax-Wendroff scheme described in section 3, like most other explicit schemes for primitive-equation models, is subject to a severe stability criterion (see equation (3.16)). This stability criterion is dominated by the speed of the fast-moving gravity waves which themselves form only an insignificant part of the pressure amplitude of synoptic-scale weather disturbances, and allows a maximum time-step of about three minutes with a = 100 km. With a stable algorithm, time integrations in steps of about 15 minutes, with a = 100 km, could proceed many times faster and would still give sufficiently accurate predictions. Semi-implicit methods belong to this category, since they are not subject to the same severe stability criteria. The essential difference between explicit and implicit schemes is most easily understood by considering some time-stepping schemes for the equation

$$\frac{\partial X}{\partial t} = \mathrm{F}(X).$$

The centred scheme $X^{n+1} = X^{n-1} + 2\,\delta t\,\mathrm{F}(X^n)$ defines X^{n+1} explicitly in terms of values at earlier time levels, whereas the scheme $X^{n+1} = X^n + \frac{\delta t}{2}(\mathrm{F}(X^n) + \mathrm{F}(X^{n+1}))$ defines X^{n+1} implicitly in terms of itself and in terms of earlier values, and X^{n+1} is subsequently determined by an inversion which usually involves the inversion of a matrix either by a direct or by an iterative method. Implicit schemes can be designed to be unconditionally stable for

particular choices of $F(X)$, but more arithmetic operations are necessary for each time-step because of the extra matrix inversion. Semi-implicit methods for primitive-equation models usually involve the implicit treatment of the terms in the model's equations that are mainly responsible for governing the motion of the gravity waves and these schemes can be designed so that the stability criteria depend on the wind speed, thus allowing a much larger time-step. The implicit scheme that has been designed for the 10-level model is based on the method of splitting, a technique pioneered mainly by Russian meteorologists, particularly Marchuk (see Marchuk *et alii* (1968)). A novel feature of the scheme is the implicit treatment of only two gravity waves compared with other schemes, for example Robert, Henderson and Turnbull (1972), which treat all the gravity waves implicitly; this feature considerably enhances efficiency by reducing the size of the inversions that are necessary for each time-step.

4.2. *The split time-stepping scheme*

Let $\mathbf{Z}_n$ be a vector whose components are all the grid-point values of the dependent variables after a complete integration cycle, where the model's equations are represented by

$$\frac{\partial \mathbf{Z}}{\partial t} + \mathbf{f} = \mathbf{s}. \qquad \ldots (4.1)$$

We define a splitting of **f** into **a** + **d** + **l**, where **a** represents the non-linear 'advective terms', **d** the frictional and diffusion terms, **l** the pressure-gradient, topographic, Coriolis and divergence or vertical-velocity terms in the thermodynamic and 1000-mb height-tendency equations, and **s** includes the source/sink terms Q and W. Explicit expressions for **a** and **l** are given below. The **l** term contains the terms mainly responsible for gravity-wave generation. The main parts of the integration cycle are advection and adjustment.

(a) *The advection stage*

Here we integrate forward in time through a single time-step, δt, the equations

$$\frac{\partial \mathbf{Z}}{\partial t} + \mathbf{a} + \mathbf{d} = 0, \qquad \ldots (4.2)$$

using the two-step Lax-Wendroff scheme described in section 3 for the advection term, **a**, with the grids shown in Figure 4.

The frictional and diffusion terms in **d** are included using a forward time-step as described in sections (3.7) and (3.8). The following values of K are used in the diffusion term (units are $m^2\ s^{-1}$). Note that the octagon value is smaller than for the Lax-Wendroff scheme.

Octagon $K = \begin{cases} 250H & \text{north of } 21^\circ\text{N, where } H \text{ is the topography height in metres} \\ 3 \times 10^6 & \text{south of } 21^\circ\text{N.} \end{cases}$

Rectangle $K = \begin{cases} 10^5 + 250H & \text{except in boundary zone} \\ 10^6 & \text{within 3 grid lengths of the lateral boundary.} \end{cases}$

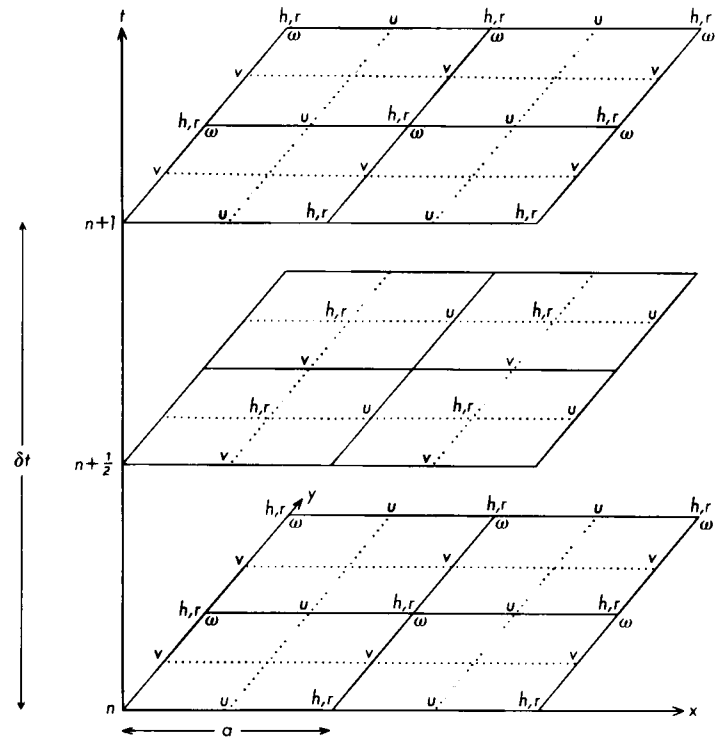

FIGURE 4. An *x-y-t* diagram illustrating the space and time staggering of the Eliassen grid, used for the advection step of the split scheme.

The advection stage of the split scheme is therefore defined by

$$\mathbf{Z}_{n+½} = \overline{\mathbf{Z}}_n^{xy} + ½\delta t(\dot{\mathbf{Z}}_A)_n \qquad \ldots (4.3)$$

$$\hat{\mathbf{Z}}_{n+1} = \mathbf{Z}_n + \delta t(\dot{\mathbf{Z}}_A)_{n+½} + \delta t(\dot{\mathbf{Z}}_F)_n + \delta t(\dot{\mathbf{Z}}_D)_n. \qquad \ldots (4.4)$$

The finite-difference approximations for $(\dot{\mathbf{Z}}_A)_n$ and $(\dot{\mathbf{Z}}_A)_{n+½}$, the tendencies due to advection, are described below in section (4.3); the approximations for $(\dot{\mathbf{Z}}_D)_n$ and $(\dot{\mathbf{Z}}_F)_n$ are those of sections (3.8) and (7.1). We can formally represent this part of the integration cycle by the matrix equation

$$\hat{\mathbf{Z}}_{n+1} = (\underline{\underline{I}} + \underline{\underline{N}})\mathbf{Z}_n \qquad \ldots (4.5)$$

where $\underline{\underline{N}}$ is the matrix operator representing the advective, frictional and diffusive changes and $\underline{\underline{I}}$ is the identity matrix.

(b) *The adjustment step*

This involves integrating

$$\frac{\partial \mathbf{Z}}{\partial t} + \mathbf{I} = 0 \qquad \ldots (4.6)$$

through a single time-step, δt, with initial conditions $\hat{\mathbf{Z}}_{n+1}$, the value of $\mathbf{Z}$ after the advective stage, using the implicit/explicit time-stepping scheme described in section (4.4) below. The state of the model atmosphere after this stage can be expressed as

$$\mathbf{Z}_{n+1} = (\underline{\underline{I}} + \underline{\underline{L}})\hat{\mathbf{Z}}_{n+1}$$

that is

$$\mathbf{Z}_{n+1} = (\underline{\underline{I}} + \underline{\underline{L}})(\underline{\underline{I}} + \underline{\underline{N}})\mathbf{Z}_n, \qquad \ldots (4.7)$$

where $\underline{\underline{L}}$ is the operator representing the changes due to the I term. The effects of the source/sink term s are now introduced to further modify $\mathbf{Z}_{n+1}$.

4.3. *Finite-difference approximations to the advective terms*

The component parts of $(\dot{\mathbf{Z}}_A)_n$ are given by

$$\dot{u}^* = \mu[\overline{u^*}^{xy}\delta_x \overline{u^*}^{y} + v^*\delta_y \overline{u^*}^{x}] - \overline{\omega}^{yp}\delta_p \overline{\overline{u^*}^{xy}}^{p} - \tfrac{1}{2}[(\overline{u^*}^{xy})^2 + (v^*)^2]\delta_x \mu \qquad \ldots (4.8)$$

$$\dot{v}^* = -\mu[u^*\delta_x \overline{v^*}^{y} + \overline{v^*}^{xy}\delta_y \overline{v^*}^{x}] - \overline{\omega}^{xp}\delta_p \overline{\overline{v^*}^{xy}}^{p} - \tfrac{1}{2}[u^{*2} + (\overline{v^*}^{xy})^2]\delta_y \mu \qquad \ldots (4.9)$$

$$\dot{h}' = -\mu(\overline{u^*}^{yp}\delta_x \overline{h'}^{y} + \overline{v^*}^{xp}\delta_y \overline{h'}^{x}) \qquad \ldots (4.10)$$

$$\dot{r} = -\mu(\overline{u^*}^{yp}\delta_x r^{y} + \overline{v^*}^{xp}\delta_y \overline{r}^{x}) - \overline{\omega}^{xp}\delta_p \overline{r}^{xy^{p}} \qquad \ldots (4.11)$$

$$\dot{h}_{10} = -\mu(\overline{u^*_{10}}^{y}\delta_x \overline{h_{10}}^{y} + \overline{v^*_{10}}^{x}\delta_y \overline{h_{10}}^{x}). \qquad \ldots (4.12)$$

Equations (4.8) to (4.12) may also be used for the second step to compute $(\dot{\mathbf{Z}}_A)_{n+\frac{1}{2}}$ except that $\overline{\omega_n}^{xp}$, $\overline{\omega_n}^{yp}$ and ω_n replace the ω terms in equations (4.8), (4.9) and (4.11) respectively. The spatial arrangement of the dependent variables for the advective step is shown in Figures 3 and 4. At the upper and lower boundaries the procedures described in section 3 are adopted. At the lateral boundaries the special measures described in section 3.9 are used for the octagon model. In the rectangle model no special procedures are necessary, since the tendencies of the outermost 'ring' of normal velocities are specified from an octagon forecast and the boundary tangential velocities are specified by internal values (see section 5 below).

4.4. *The finite-difference approximations for the adjustment step*

The prognostic equations for the adjustment step are

$$\frac{\partial u^*}{\partial t} - fv^* + g\frac{\partial h}{\partial x} = 0 \qquad \ldots (4.13)$$

$$\frac{\partial v^*}{\partial t} + fu + g\frac{\partial h}{\partial y} = 0 \qquad \ldots (4.14)$$

$$\frac{\partial h'}{\partial t} + \beta\omega = 0 \qquad \ldots (4.15)$$

$$\frac{\partial \omega_{10}}{\partial t} + \left(\frac{\partial h}{\partial p}\right)_{10} \omega_{10} - \mu\left(u_{10}\frac{\partial H}{\partial x} + v_{10}\frac{\partial H}{\partial y}\right) = 0. \qquad \ldots (4.16)$$

The equations (4.13) to (4.16) define **l** in equation (4.6). For our purpose it is convenient to define the 10-dimensional column vectors

$$\mathbf{u} = \begin{pmatrix} u^*_1 \\ \vdots \\ u^*_{10} \end{pmatrix}, \quad \mathbf{v} = \begin{pmatrix} v^*_1 \\ \vdots \\ v^*_{10} \end{pmatrix} \quad \mathbf{h} = \begin{pmatrix} h_1 \\ \vdots \\ h_{10} \end{pmatrix} \quad \text{and } \omega = \begin{pmatrix} \omega_{1+\frac{1}{2}} \\ \vdots \\ \omega_{9+\frac{1}{2}} \\ \omega_{10} \end{pmatrix}$$

and recast equations (4.13) to (4.16) in the 'vector' form

$$\frac{\partial \mathbf{u}}{\partial t} - f\mathbf{v} + g\frac{\partial \mathbf{h}}{\partial x} = 0 \qquad \ldots (4.17)$$

$$\frac{\partial \mathbf{v}}{\partial t} + f\mathbf{u} + g\frac{\partial \mathbf{h}}{\partial y} = 0 \qquad \ldots (4.18)$$

$$\underline{\underline{A}}\frac{\partial \mathbf{h}}{\partial t} + \underline{\underline{B}}\omega + \mu\,\underline{\underline{T}}_o\left(\frac{\partial H}{\partial x}\mathbf{u} + \frac{\partial H}{\partial y}\mathbf{v}\right) = 0 \qquad \ldots (4.19)$$

where the 10 x 10 matrices $\underline{\underline{A}}$, $\underline{\underline{B}}$ and $\underline{\underline{T}}_o$ are given by

$$A = \begin{pmatrix} 1 & -1 & & & & & & & & 0 \\ & 1 & -1 & & & & & & & \\ & & \ddots & \ddots & & & & & & \\ & & & \ddots & \ddots & & & & & \\ & & & & \ddots & \ddots & & & & \\ & & & & & \ddots & \ddots & & & \\ & & & & & & \ddots & \ddots & & \\ & & & & & & & 1 & -1 & \\ 0 & & & & & & & & 1 & \end{pmatrix}$$

$\underline{\underline{B}}$ = diag $(\beta_{1+\frac{1}{2}}, \text{-----}, \beta_{9+\frac{1}{2}}, -h'_{9+\frac{1}{2}}/\Delta p)$, and

$\underline{\underline{T}}_o$ = diag (0,0,0,0,0,0,0,0,0,-1). The vertically integrated vector form of the continuity equation (2.4) may be written

$$\underline{\underline{A}}^T\omega = -\mu\Delta p\,\underline{\underline{D}}\left(\frac{\partial \mathbf{u}}{\partial x} + \frac{\partial \mathbf{v}}{\partial y}\right), \qquad \ldots (4.20)$$

where $\underline{\underline{D}}$ = diag (1,1,1,1,1,1,1,1,1,½).

The elimination of ω between (4.19) and (4.20) gives

$$\frac{\partial \mathbf{h}}{\partial t} + \frac{\mu}{g}\underline{\underline{G}}\left(\frac{\partial \mathbf{u}}{\partial x} + \frac{\partial \mathbf{v}}{\partial y}\right) + \mu\,\underline{\underline{T}}\left(\frac{\partial H}{\partial x}\mathbf{u} + \frac{\partial H}{\partial y}\mathbf{v}\right) = 0 \qquad \ldots (4.21)$$

where $\underline{\underline{G}} = -g\Delta p\,\underline{\underline{A}}^{-1}\,\underline{\underline{B}}(\underline{\underline{A}}^T)^{-1}\,\underline{\underline{D}}$ and $\underline{\underline{T}} = \underline{\underline{A}}^{-1}\,\underline{\underline{T}}_o$.

We rewrite (4.21) as

$$\frac{\partial \mathbf{h}}{\partial t} + \frac{\mu}{g}\underline{\underline{G}}_0\left(\frac{\partial \mathbf{u}}{\partial x} + \frac{\partial \mathbf{v}}{\partial y}\right) + \frac{\mu}{g}(\underline{\underline{G}} - \underline{\underline{G}}_0)\left(\frac{\partial \mathbf{u}}{\partial x} + \frac{\partial \mathbf{v}}{\partial y}\right) + \mu\underline{\underline{T}}\left(\frac{\partial H}{\partial x}\mathbf{u} + \frac{\partial H}{\partial y}\mathbf{v}\right) = 0, \quad \ldots (4.22)$$

where $\underline{\underline{G}}_0$ is an ICAO matrix corresponding to ICAO values of the $\beta_{k+\frac{1}{2}}$ and $h'_{9+\frac{1}{2}}/\Delta p$. We define new velocities and heights by the linear transformations

$$\mathbf{a} = \underline{\underline{E}}^{-1}\mathbf{u}$$

$$\mathbf{b} = \underline{\underline{E}}^{-1}\mathbf{v}$$

$$\mathbf{y} = \underline{\underline{E}}^{-1}\mathbf{h}$$

and choose $\underline{\underline{E}}$ to be the matrix whose columns are the right-hand eigenfunctions of the ICAO matrix $\underline{\underline{G}}_0$.

The new variables satisfy

$$\frac{\partial a_k}{\partial t} + g\frac{\partial y_k}{\partial x} = f b_k \quad \ldots (4.23)$$

$$\frac{\partial b_k}{\partial t} + g\frac{\partial y_k}{\partial y} = -f a_k \quad \ldots (4.24)$$

$$\frac{\partial y_k}{\partial t} + \frac{\mu C_k^2}{g}\left(\frac{\partial a_k}{\partial x} + \frac{\partial b_k}{\partial y}\right) = -\left\{\underline{\underline{E}}^{-1}\left[\frac{\mu}{g}(\underline{\underline{G}} - \underline{\underline{G}}_0)\left(\frac{\partial \mathbf{u}}{\partial x} + \frac{\partial \mathbf{v}}{\partial y}\right) + \mu\underline{\underline{T}}\left(\mathbf{u}\frac{\partial H}{\partial x} + \mathbf{v}\frac{\partial H}{\partial y}\right)\right]\right\}_k \quad \ldots (4.25)$$

where $k = 1, ----, 10$, and $C_k^2 = (\underline{\underline{E}}^{-1}\,\underline{\underline{G}}_0\underline{\underline{E}})_k$ are the eigenvalues of $\underline{\underline{G}}_0$, which we order so that $C_k > C_{k+1}$. The ten values of C_k for an ICAO atmosphere are given in Table 1. If we drop the right-hand sides of equations (4.23) to (4.25) then these equations describe the motion of small-amplitude gravity waves in the model in a stratified fluid. For the eight slowest-moving modes we use the explicit scheme

$$(a_k)_{n+1} - (a_k)_n = -\delta_{tg}\delta_x(y_k)_{n+1} + \delta t f(\bar{b}_k^{xy})_n, \quad \ldots (4.26)$$

$$(b_k)_{n+1} - (b_k)_n = -\delta tg\delta_y(y_k)_{n+1} - \delta t f(\bar{a}_k^{xy})_n, \quad \ldots (4.27)$$

$$(y_k)_{n+1} - (y_k)_n = -\delta t\frac{\mu}{g}C_k^2(\delta_x a_k + \delta_y b_k)_n + \Delta y_k, \quad \ldots (4.28)$$

where

$$\Delta y_k = -\delta t\left\{\underline{\underline{E}}^{-1}\left[\frac{\mu}{g}(\underline{\underline{G}} - \underline{\underline{G}}_0)(\delta_x\mathbf{u} + \delta_y\mathbf{v}) + \mu\underline{\underline{T}}(\delta_x\bar{H}^{xyy})\bar{\mathbf{u}}^x + (\delta_y\bar{H}^{xyx})\bar{\mathbf{v}}^y\right]\right\}_k \quad \ldots (4.29)$$

for $k = 3, 4, \ldots, 9, 10$.

For $k = 1, 2$ we use the following semi-implicit scheme.

$$(a_k)_{n+1} - (a_k)_n = -\frac{\delta tg}{2}(\delta_x(y_k)_n + \delta_x(\hat{y}_k)_{n+1}) - \delta tg\delta_x(y'_k)_{n+1} + \delta t f(\bar{b}_k^{xy})_n \quad \ldots (4.30)$$

$$(b_k)_{n+1} - (b_k)_n = -\frac{\delta tg}{2}(\delta_y(\gamma_k)_n + \delta_y(\tilde{\gamma}_k)_{n+1}) - \delta tg\delta_y(\gamma'_k)_{n+1} - \delta tf(\bar{a}_k^{xy})_n \quad \ldots (4.31)$$

$$(\gamma_k)_{n+1} - (\gamma_k)_n = -\frac{\delta t}{2}\mu\frac{C_k^2}{g}(\delta_x(a_k)_n + \delta_y(b_k)_n + \delta_x(a_k)_{n+1} + \delta_y(b_k)_{n+1}) + \Delta\gamma_k, \quad \ldots (4.32)$$

where

$$(\gamma'_k)_{n+1} = -\delta t\left\{\underline{\underline{E}}^{-1}\left[\frac{\mu}{g}(\underline{\underline{G}}_n - \underline{\underline{G}}_o)(\delta_x \mathbf{u} + \delta_y \mathbf{v})\right]\right\}_k \quad \ldots (4.33)$$

and

$$(\tilde{\gamma}_k)_{n+1} = (\gamma_k)_{n+1} - (\gamma'_k)_{n+1}. \quad \ldots (4.34)$$

If we introduce $(\psi_k)_{n+1} = (\gamma_k)_n + (\tilde{\gamma}_k)_{n+1} + 2(\gamma'_k)_{n+1} = (\gamma_k)_n + (\gamma_k)_{n+1} + (\gamma'_k)_{n+1}$ and eliminate $(a_k)_{n+1}$ and $(b_k)_{n+1}$ from equations (4.30), (4.31) and (4.32) we obtain the Helmholtz equations

$$-\nabla^2(\psi_k)_{n+1} + \frac{4}{\mu\delta t^2 C_k^2}(\psi_k)_{n+1} = \frac{4}{\mu\delta t^2 C_k^2}\left[f_k - \frac{\delta t}{2}\mu\frac{C_k^2}{g}\left\{\delta_x(\delta tf\bar{b}_k^{xy})_n + \delta_y(-\delta tf\bar{a}_k^{xy})_n\right\}\right] \quad \ldots (4.35)$$

with

$$\nabla^2 \equiv \delta_x\delta_x + \delta_y\delta_y,$$

and

$$f_k = 2(\gamma_k)_n + \Delta\gamma_k + (\gamma'_k)_n - \delta t\,\mu\frac{C_k^2}{g}(\delta_x a_k + \delta_y b_k)_n \text{ for } k = 1, 2. \quad \ldots (4.36)$$

Once $(\psi_k)_{n+1}$ has been determined from (4.35), with $(\psi_k)_{n+1}$ specified on the boundaries, we obtain $(\gamma_k)_{n+1}$ from

$$(\gamma_k)_{n+1} = (\psi_k)_{n+1} - (\gamma_k)_n - (\gamma'_k)_{n+1},$$

that is

$$(\gamma_k)_{n+1} = (\gamma_k)_n - \delta t\,\mu\frac{C_k^2}{g}(\delta_x a_k + \delta_y b_k)_n + \Delta\gamma_k + \{(\psi_k)_{n+1} - f_k\}. \quad \ldots (4.37)$$

From (4.37) we see that for $k = 1, 2$, $(\gamma_k)_{n+1}$ is given by the explicit forward time-step of the scheme in equation (4.28) plus the 'correction' $(\psi_k)_{n+1} - f_k$ and combining (4.28) and (4.37) we can write

$$\mathbf{y}_{n+1} = \mathbf{y}_n - \frac{\delta t}{g}\mu\,\underline{\underline{C}}_o^2(\delta_x \mathbf{a} + \delta_y \mathbf{b})_n + \Delta\mathbf{y} + ((\psi_1)_{n+1} - f_1)\,\mathbf{e}_1 + ((\psi_2)_{n+1} - f_2)\,\mathbf{e}_2 \quad \ldots (4.38)$$

where

$$\mathbf{e}_1 = \begin{pmatrix} 1 \\ 0 \\ \vdots \\ 0 \end{pmatrix} \quad \text{and} \quad \mathbf{e}_2 = \begin{pmatrix} 0 \\ 1 \\ 0 \\ \vdots \\ 0 \end{pmatrix},$$

and $\underline{\underline{C}}_o^2 = \text{diag}\,(C_1^2, \cdots, C_9^2, C_{10}^2)$.

Multiplying (4.38) by $\underline{\underline{E}}$ gives

$$\mathbf{h}_{n+1} = \mathbf{h}_n - \frac{\delta t}{g}\mu\, \underline{\underline{G}}_o\, (\delta_x \mathbf{u} + \delta_y \mathbf{v})_n + \Delta\mathbf{h} + ((\psi_1)_{n+1} - f_1)\,\hat{\mathbf{y}}_1 + ((\psi_2)_{n+1} - f_2)\,\hat{\mathbf{y}}_2 =$$

$$= \mathbf{h}^* + ((\psi_1)_{n+1} - f_1)\,\hat{\mathbf{y}}_1 + ((\psi_2)_{n+1} - f_2)\,\hat{\mathbf{y}}_2\,, \qquad \ldots (4.39)$$

$$\mathbf{h}^* = \mathbf{h}_n - \frac{\delta t}{g}\mu\, \underline{\underline{G}}_o\, (\delta_x \mathbf{u} + \delta_y \mathbf{v}) + \Delta\mathbf{h}$$

and $\Delta\mathbf{h} = \underline{\underline{E}}\,\Delta\,\mathbf{y} = -\delta t \left\{\left[\frac{\mu}{g}(\underline{\underline{G}}_n - \underline{\underline{G}}_o)(\delta_x \mathbf{u} + \delta_y \mathbf{v})_n + \mu\, \underline{\underline{T}}\,(\delta_x \bar{H}^{xyy}\,\bar{u}^x + \delta_y \bar{H}^{xyx}\,\bar{v}^y)_n\right]\right\}$

and $\hat{y}_k = \underline{\underline{E}}\,\mathbf{e}_k$, $k = 1, 2$, are the first two eigenfunctions of $\underline{\underline{G}}_o$ according to the ordering prescribed above for the eigenvalues.

The computation cycle is summarized as follows:

(i) $\mathbf{h}^*$, $\Delta_1\,\mathbf{h} = -\delta t \left\{\frac{\mu}{g}(\underline{\underline{G}}_n - \underline{\underline{G}}_o)(\delta_x \mathbf{u} + \delta_y \mathbf{v})\right\}$, $\Delta_c\,\mathbf{u}_n = \delta t f\,\bar{\mathbf{v}}^i_{n+\frac{1}{2}}$ and $\Delta_c\,\mathbf{v}_n = -\delta t f\,\bar{\mathbf{u}}^i_{n+\frac{1}{2}}$ are obtained by explicit operations. $\bar{\mathbf{u}}^i_{n+\frac{1}{2}}$ and $\bar{\mathbf{v}}^i_{n+\frac{1}{2}}$ are designed to provide second order accuracy in time in the Coriolis terms and are given by

$$\bar{\mathbf{u}}^i_{n+\frac{1}{2}} = \bar{\mathbf{u}}^i_n - \frac{\delta t}{2}\,(f\mathbf{v}_n + g\,\overline{\delta x\, h_n}^{xy})$$

$$\bar{\mathbf{v}}^i_{n+\frac{1}{2}} = \bar{\mathbf{v}}^i_n - \frac{\delta t}{2}\,(-f\bar{\mathbf{u}}_n^{xy} + g\,\overline{\delta y\, h_n}^{xy}).$$

$\bar{\mathbf{u}}^i_n$ and $\bar{\mathbf{v}}^i_n$ are horizontally interpolated values; in the rectangle $\bar{\mathbf{u}}^i_n = \bar{\mathbf{u}}^{xy}_n$, $\bar{\mathbf{v}}^i_n = \bar{\mathbf{v}}^{xy}_n$, but in the octagon bicubic interpolations are used.

(ii) Compute $f_k = \hat{\mathbf{X}}_k^{\mathrm{T}} \cdot (\mathbf{h}^* + \mathbf{h}_n + \Delta_1\mathbf{h})$ $k = 1, 2$ where $\mathbf{X}_k^{\mathrm{T}}$ is the kth row of $\underline{\underline{E}}^{-1}$.

(iii) Compute

$$f_k - \hat{\mathbf{X}}_k^{\mathrm{T}} \cdot \frac{\delta t}{2}\frac{\mu}{g}\underline{\underline{G}}_o\,(\delta_x\,(\Delta_c\,\mathbf{u}_n) + \delta_y\,(\Delta_c\,\mathbf{v}_n)) =$$

$$= f_k - \frac{\delta t}{2}\,\mu\,\frac{C_k^2}{g}\,(\delta_x\,(\delta t f \bar{b}_k^{xy}) + \delta_y\,(-\delta t f \bar{a}_k^{xy})),$$

the right-hand sides of the Helmholtz equations (4.35).

(iv) Solve the Helmholtz equations (4.35) for $(\psi_1)_{n+1}$ and $(\psi_2)_{n+1}$; f_k is a good first guess for $(\psi_k)_{n+1}$ in the iterative alternating-direction implicit method used to solve those equations.

(v) Adjust $\mathbf{h}^*$ according to equation (4.39) to give $\mathbf{h}_{n+1}$.

(vi) $\mathbf{u}_{n+1}$ and $\mathbf{v}_{n+1}$ are then given by

$$\mathbf{u}_{n+1} = \mathbf{u}_n - \delta t g \delta_x \mathbf{h}_{n+1} - \frac{\delta t}{2} g \left\{ 2\delta_x ((y_1)_{n+1} + (y'_1)_{n+1}) - \delta_x (\psi_1)_{n+1} \right\} \hat{y}_1 -$$

$$- \frac{\delta t}{2} g \left\{ 2\delta_x ((y_2)_{n+1} + (y'_2)_{n+1}) - \delta_x (\psi_2)_{n+1} \right\} \hat{y}_2 + \Delta_c \mathbf{u}_n \qquad \ldots (4.40)$$

and

$$\mathbf{v}_{n+1} = \mathbf{v}_n - \delta t g \delta_y \mathbf{h}_{n+1} - \frac{\delta t}{2} g \left\{ 2\delta_y ((y_1)_{n+1} + (y'_1)_{n+1}) - \delta_y (\psi_1)_{n+1} \right\} \hat{y}_1 -$$

$$- \frac{\delta t}{2} g \left\{ 2\delta_y ((y_2)_{n+1} + (y'_1)_{n+1} - \delta_y (\psi_2)_{n+1} \right\} \hat{y}_2 + \Delta_c \mathbf{v}_n. \qquad \ldots (4.41)$$

4.4. *Computational stability of the split scheme*

The split scheme, described by equation 4.7 is stable provided that each stage of the integration cycle is stable. A linearized analysis similar to the one described in section 3 can be made for each stage and provides necessary conditions for stability.

The linearized equations for the advection step, leaving out the frictional and diffusion terms, are of the form

$$\frac{\partial Z}{\partial t} = -m \left(U \frac{\partial Z}{\partial x} + V \frac{\partial Z}{\partial y} \right) \qquad \ldots (4.42)$$

and the explicit Lax-Wendroff treatment of this equation is stable provided that

$$\delta t < a / m \sqrt{(U^2 + V^2)}. \qquad \ldots (4.43)$$

If we neglect the Coriolis, topographic and diabatic heating terms and assume an unperturbed atmosphere with a vertical structure such that $\underline{\underline{G}} = (1 + \alpha)\, \underline{\underline{G}}_0$ for constant α, the decoupled system is then

$$\frac{\partial a_k}{\partial t} = -mg \frac{\partial y_k}{\partial x}, \qquad \ldots (4.44)$$

$$\frac{\partial b_k}{\partial t} = -mg \frac{\partial y_k}{\partial y}, \qquad \ldots (4.45)$$

$$\frac{\partial y_k}{\partial t} = -\frac{m}{g} C_k^2 \left(\frac{\partial a_k}{\partial x} + \frac{\partial b_k}{\partial y} \right) - \frac{m\alpha}{g} C_k^2 \left(\frac{\partial a_k}{\partial x} + \frac{\partial b_k}{\partial y} \right) \qquad \ldots (4.46)$$

For $k = 3, \cdots, 10$ the explicit scheme described by equations (4.26) is used and is stable provided that

$$\Delta t < \text{minimum}_{k=3,\cdots,10} \left\{ a/C_k m \sqrt{2(1+\alpha)} \right\} = a/C_3 m \sqrt{2(1+\alpha)}. \quad \ldots (4.47)$$

For $k = 1, 2$ the semi-explicit scheme described by equations (4.30) to (4.34) is used and is unconditionally stable for zero or negative α and is stable provided that

$$\delta t < a/C_k m \sqrt{2\alpha} \quad \ldots (4.48)$$

for positive α, where $k = 1, 2$. If values of $\sqrt{(U^2 + V^2)}$ equal to or greater than 100 m s^{-1} are allowed for, then the criterion of equation (4.43) provides the most severe restriction and allows a much longer time-step than (3.16). A final point on stability; in order to avoid the occasional occurrences of excessive small-scale roughnesses, particularly over sea areas, the heating due to surface transfers is included in the adjustment step by adding the appropriate source vector to the right-hand side of (4.39).

In the rectangle we use a 12-minute time-step and this allows for values of $\sqrt{(U^2 + V^2)}$ up to 100 m s^{-1}. In the octagon values of $\sqrt{(U^2 + V^2)}$ up to 150 m s^{-1} are to be allowed for, and this restricts the time-step to about 24 minutes. In fact the time-step used is 15 minutes because of the severe time-truncation of the split time-stepping scheme, which is only a first-order scheme in δt.

TABLE I. *The phase speeds of the model's gravity waves for an ICAO atmosphere*

k	1	2	3	4	5	6	7	8	9	10
C_k (m s^{-1})	298	99	47	30	19	13	10	8	7	5

5. LATERAL BOUNDARY CONDITIONS

In the octagon model the boundary heights, humidity mixing ratios and velocities are kept constant throughout the forecast period. Control of the boundary instabilities that generally arise because of this over-specification of boundary conditions is maintained by the use of an enhanced horizontal diffusion coefficient in a narrow boundary zone (see section 3.8) and the special measures described in section 3.9.

In the rectangle the boundary heights (h_b), humidity mixing ratios (r_b) and normal velocities (V_{bN}) are given by

$$(h_b)_{n+1} = (h_b)_n + \delta t \left(\frac{\partial (h_b)_n}{\partial t} \right)_8$$

$$(r_b)_{n+1} = (r_b)_n + \delta t \left(\frac{\partial (r_b)_n}{\partial t}\right)_8$$

$$(V_{bN})_{n+1} = (V_{bN})_n + \delta t \left(\frac{\partial (V_{bN})_n}{\partial t}\right)_8$$

where the suffix b refers to boundary values, and $(\partial\ (h_b)_n/\partial t)_8$ etc. are the interpolated octagon forecast tendencies for the rectangle boundary. In the semi-implicit model V_{bN} refers to the outermost 'ring' of normal velocities. The boundary tangential velocities, V_{bT} for the semi-implicit model are determined from internal values according to the relation

$$(V_{bT})_{n+1} = (V_{bT})_n + \{(V_{b-1T})_{n+1} - (V_{b-1T})_n\},$$

where the V_{b-1T} are values at the neighbouring internal points. Stability at the boundaries is again maintained by using an enhanced diffusion coefficient within a narrow boundary zone.

6. PRECIPITATION PROCESSES

6.1. *Introduction*

In this section the procedures for calculating the contributions to Q and W from the condensation and sublimation of water vapour and the evaporation of precipitation are described. The precipitation in the 100-mb layers above the melting level, which is taken to be the height of the highest 0°C isotherm, is assumed to be snow which melts in the layer containing the melting level to form rain. At temperatures higher than 268 K precipitation is produced at a sufficient rate to keep the air saturated at saturation over liquid water wherever supersaturation would otherwise occur. At temperatures lower than 268 K snowflakes are grown at a humidity intermediate between water- and ice-saturation. These assumptions are strongly supported by a study made by Wexler (1952) and this scheme provides a simple but reasonable description of the observed vertical structure of the precipitation falling from thick stratiform clouds in middle latitudes.

It is necessary to test each 100-mb layer (below 300 mb) for saturation with respect to liquid water or ice and this is done by comparing the humidity mixing ratio, r, representative of the layer with the appropriate saturation mixing ratio, r_s. For

$$T_{k+\frac{1}{2}} = gh'_{k+\frac{1}{2}}/R \log_e(k + 1/k)$$

greater than or equal to 268 K, $(r_s)_{k+\frac{1}{2}}$ is determined from the quartic polynomial $G^W{}_{k+\frac{1}{2}}$ in the thickness $h'_{k+\frac{1}{2}}$, whilst for $T_{k+\frac{1}{2}}$ less than 268 K, r_s is determined from the quartic $G^I{}_{k+\frac{1}{2}}$. The coefficients for the seven polynomials $G^W{}_{k+\frac{1}{2}}$, $k = 1, 2, \cdots 9$, were obtained by fitting a quartic to the saturation humidity mixing ratio over water, which can be expressed as an implicit function of the layer thickness, by the method of least squares. The coefficients for the polynomials $G^I{}_{k+\frac{1}{2}}$ were obtained by a least-squares fit to the saturation humidity mixing ratio over ice for $T_{k+\frac{1}{2}} < 268$ K, subject to the two conditions

$$\left.\begin{aligned} G^I{}_{k+\frac{1}{2}} &= G^W{}_{k+\frac{1}{2}} \\ \mathrm{d}/\mathrm{d}h'_{k+\frac{1}{2}}\ G^I{}_{k+\frac{1}{2}} &= \mathrm{d}/\mathrm{d}h'_{k+\frac{1}{2}}\ G^W{}_{k+\frac{1}{2}} \end{aligned}\right\} \quad \text{at } T_{k+\frac{1}{2}} = 268 \text{ K}.$$

The coefficients obtained are listed in Table II.

Three assumptions which are implied in the formulation should be noted:

(i) No condensation or sublimation takes place as a result of large-scale motions (as distinct from small-scale convective motions) until the air becomes saturated on the grid scale.

(ii) condensation or sublimation takes place at a sufficient rate to keep the air exactly saturated whenever supersaturation would otherwise occur.

(iii) There is no storage of liquid water in the model atmosphere, so that any liquid water or snow produced as a result of condensation or sublimation falls immediately through the layers below, is modified by evaporation if any of these layers is unsaturated, and may reach the 1000-mb level where it is interpreted as surface precipitation distributed over the whole time-step.

6.2. *Condensation or sublimation of water vapour*

Let $[r]_{k+½}$ and $[h']_{k+½}$ be the humidity mixing ratio and the thickness of layer $k+½$ obtained at time $t + \delta t$ with no account taken of condensation or sublimation and evaporation during the time interval $(t, t + \delta t)$ and that $[r_s]_{k+½}$ is the saturation mixing ratio obtained from $[h']_{k+½}$ using the appropriate quartic polynomial. If $[r]_{k+½} \leqslant [r_s]_{k+½}$ no action is taken. If, however, $[r]_{k+½} > [r_s]_{k+½}$, adjusted values $r_{k+½}$ and $h'_{k+½}$ are obtained such that $r_{k+½} = (r_s)_{k+½}$ where $(r_s)_{k+½}$ is the saturation mixing ratio corresponding to $h'_{k+½}$. In order to take account of the effects of latent-heat release on the thickness of the layer, $r_{k+½}$ and $h'_{k+½}$ are obtained by solving simultaneously the heat conservation equation

$$c_p\,(T_{k+½} - [T]_{k+½}) = L\,([r]_{k+½} - (r_s)_{k+½}), \qquad \ldots (6.2)$$

and the finite-difference form of the Clausius-Clapeyron equation

$$\frac{(r_s)_{k+½} - [r_s]_{k+½}}{T_{k+½} - [T]_{k+½}} = \frac{\epsilon L [r_s]_{k+½}}{R[T]^2_{k+½}}, \qquad \ldots (6.3)$$

where L is the appropriate latent heat, $[T]_{k+½}$ and $T_{k+½}$ are values at $t + \delta t$ before and after adjustment, and are given by equations such as (6.1). After a little algebra these equations give the relationship

$$h'_{k+½} = [h']_{k+½} + \frac{R}{g} \log_e \frac{k+1}{k} \frac{L([r]_{k+½} - [r_s]_{k+½})}{c_p + (\epsilon L^2 R / g[h']^2_{k+½}) \log_e^2 (k+1/k)\,[r_s]_{k+½}} \qquad \ldots (6.4)$$

The adjusted humidity mixing ratio $r_{k+½} = (r_s)_{k+½}$ is then obtained from $h'_{k+½}$ by using the quartic polynomial. If M_k is the mixing ratio of precipitation transferred from layer $k-½$ to $k+½$ during the time interval $(t, t + \delta t)$, then

$$M_{k+1} = M_k + [r]_{k+½} - (r_s)_{k+½}. \qquad \ldots (6.5)$$

If $r_{k+½}$ and $h'_{k+½}$ obtained from equations (6.10) and (6.11) imply supersaturation, a solution such that $r_{k+½} = (r_s)_{k+½}$ is calculated, the required $h'_{k+½}$ being given by equation (6.4).

TABLE II. *Coefficients for the quartic polynomials* $G^{W}{}_{k+½}$ *and* $G^{I}{}_{k+½}$

Pressure (mb)		Coefficients for the 7 polynomials $G^{W}{}_{k+½}$	Coefficients for the 7 polynomials $G^{I}{}_{k+½}$
	$a^3{}_0$	$0.24294033021271 \times 10^4$	$-0.84937738293872 \times 10^3$
	$a^3{}_1$	$-0.51887906801389 \times 10^4$	$0.12665900758531 \times 10^1$
350	$a^3{}_2$	$0.41621896309729 \times 10^{-2}$	$-0.58730729779284 \times 10^{-3}$
	$a^3{}_3$	$-0.14865068105822 \times 10^{-5}$	$0.61157309432881 \times 10^{-7}$
	$a^3{}_4$	$0.19949929591638 \times 10^{-9}$	$0.11026115952975 \times 10^{-10}$
	$a^4{}_0$	$0.26302008958507 \times 10^4$	$-0.29165864758459 \times 10^4$
	$a^4{}_1$	$-0.70756930987831 \times 10^1$	$0.67642175454979 \times 10^1$
450	$a^4{}_2$	$0.71735793175904 \times 10^{-2}$	$-0.57625759975618 \times 10^{-2}$
	$a^4{}_3$	$-0.32356160609221 \times 10^{-5}$	$0.21211139849163 \times 10^{-5}$
	$a^4{}_4$	$0.54877339769525 \times 10^{-9}$	$-0.28099348988709 \times 10^{-9}$
	$a^5{}_0$	$0.26533967609099 \times 10^4$	$-0.53919568019203 \times 10^4$
	$a^5{}_1$	$-0.86296713698006 \times 10^1$	$0.15693266824421 \times 10^2$
550	$a^5{}_2$	$0.10551398266682 \times 10^{-1}$	$-0.16971086628135 \times 10^{-1}$
	$a^5{}_3$	$-0.57499100545145 \times 10^{-5}$	$0.80648184311442 \times 10^{-5}$
	$a^5{}_4$	$0.11786891251448 \times 10^{-8}$	$-0.14166817908531 \times 10^{-8}$
	$a^6{}_0$	$0.24930017562489 \times 10^4$	$-0.13177102292101 \times 10^5$
	$a^6{}_1$	$-0.95329026495835 \times 10^1$	$0.45720079069159 \times 10^2$
650	$a^6{}_2$	$0.13705709811643 \times 10^{-1}$	$-0.59259513693282 \times 10^{-1}$
	$a^6{}_3$	$-0.87833999466189 \times 10^{-5}$	$0.33986138058760 \times 10^{-4}$
	$a^6{}_4$	$0.21176796766026 \times 10^{-8}$	$-0.72714650709397 \times 10^{-8}$
	$a^7{}_0$	$0.21305969908842 \times 10^4$	$-0.15971655332488 \times 10^5$
	$a^7{}_1$	$-0.94671008759870 \times 10^1$	$0.63895988199579 \times 10^2$
750	$a^7{}_2$	$0.15802134421579 \times 10^{-1}$	$-0.95569499937271 \times 10^{-1}$
	$a^7{}_3$	$-0.11747184362993 \times 10^{-4}$	$0.63312320167505 \times 10^{-4}$
	$a^7{}_4$	$0.32828209405487 \times 10^{-8}$	$-0.15666093677744 \times 10^{-7}$
	$a^8{}_0$	$0.14765014256811 \times 10^4$	$-0.50702326071120 \times 10^5$
	$a^8{}_1$	$-0.77980088621939 \times 10^1$	$0.22829240382474 \times 10^3$
850	$a^8{}_2$	$0.15341501787956 \times 10^{-1}$	$-0.38500305527270 \times 10^0$
	$a^8{}_3$	$-0.13351128164514 \times 10^{-4}$	$0.28818849671856 \times 10^{-3}$
	$a^8{}_4$	$0.43435018080841 \times 10^{-8}$	$-0.80774610297429 \times 10^{-7}$
	$a^9{}_0$	$0.88426958965517 \times 10^3$	$-0.14892681081088 \times 10^6$
	$a^9{}_1$	$-0.58290562762517 \times 10^1$	$0.74348199606711 \times 10^3$
950	$a^9{}_2$	$0.13849113980057 \times 10^1$	$-0.13911214920348 \times 10^1$
	$a^9{}_3$	$-0.14251239998002 \times 10^{-4}$	$0.11561747502444 \times 10^{-2}$
	$a^9{}_4$	$0.54041190057713 \times 10^{-8}$	$-0.36011074736195 \times 10^{-6}$

$$G^{W,I}{}_{k+½} = \sum_{m=0}^{4} a_m{}^k \, (h'_{k+½})^m$$

6.3. *The melting of snow*

The snowflakes are melted in the highest layer whose mean virtual temperature is greater than 273 K. The change in $\Delta T_{k+½}$ produced by the melting of M_k g/kg of snow in the layer $k+½$ is given by

$$L_f M_k = -c_p \Delta T_{k+½}, \qquad \ldots (6.6)$$

where L_f is the latent heat of fusion of ice.

The corresponding change in thickness, $\Delta h'_{k+½}$ of the layer $k+½$ is given by

$$\Delta h'_{k+½} = -\frac{R}{g} \log \frac{k+1}{k} \frac{L_f}{c_p} M_k. \quad \ldots (6.7)$$

This cooling of the layer is incorporated before the layer is tested for supersaturation.

6.4. *The evaporation of precipitation*

If $[r]_{k+½} < [r_s]_{k+½}$ some or all of the precipitation, if any, falling through level k will evaporate as it falls through layer $k+½$. If the precipitation rate at the top, level k, of a subsaturated 100-mb layer is P_k mm/h then the precipitation rate at the bottom, level $k+1$, P_{k+1} mm/h, is given by

$$P^{\nu}_{k+1} - P^{\nu}_{k} = -E_{k+½}(1 - X_{k+½}) \quad \ldots (6.8)$$

where $X_{k+½}$ is the mean relative humidity of the layer and P_k is given by

$$P_k = \frac{10\Delta p}{g} M_k \frac{3600}{\delta t}. \quad \ldots (6.9)$$

The constants ν and $E_{k+½}$, $k = 4, 5, ----, 9$, are given in Table III for rain and Table IV for snow. The evaporation law is similar to one derived by Best (1952) and is based on an equation derived by Mason (1957) for the rate of growth of a spherical precipitation particle by diffusion of water vapour. Since we are concerned only with evaporation Mason's growth equation was modified to allow for ventilation effects. If P_{k+1} determined from equation (6.8) is negative then all the liquid water falling through level k is assumed to have evaporated in layer $k+½$ and $P_{k+½}$ is taken to be zero. Equation (6.5) is then replaced by

$$r_{k+½} = [r]_{k+½} + M_k - M_{k+1} \quad \ldots (6.10)$$

and $h'_{k+½}$ is given by

$$h'_{k+½} = [h']_{k+½} - \frac{R}{g} \log_e \frac{k+1}{k} \frac{L}{c_p} (M_k - M_{k+1}). \quad \ldots (6.11)$$

TABLE III. *Evaporation constants for rain*

k	4	5	6	7	8	9
$E_{k+½}$	0.1997	0.3485	0.4736	0.5600	0.7171	0.8157
			$\nu = 0.51968$			

TABLE IV. *Evaporation constants for snow*

k	4	5	6	7	8	9
$E_{k+½}$	0.923	1.765	2.492	3.208	3.853	4.368
			$\nu = 0.8685$			

7. SURFACE EXCHANGES

7.1. *Surface friction*

The exchange of momentum between the atmosphere and the underlying surface is represented by the term $-g\tau_p$ in the momentum equation (see equation (2.1)). This term is calculated in two stages as follows.†

(a) The stress vector τ_{10} at 1000 mb is evaluated using the 1000-mb velocity $\mathbf{V}_{10}$ and a conventional drag-coefficient formulation.

$$\tau_{10} = \rho_{10} C_D |\mathbf{V}_{10}| \mathbf{V}_{10} . \qquad \ldots (7.1)$$

The ICAO standard atmosphere 1000-mb value is used for ρ_{10}.

The values of C_D used in the model are as follows.

$$\begin{aligned} C_D &= 1.0 \times 10^{-3} && \text{over sea.} \\ C_D &= \left(1.0 + \frac{H}{400}\right) \times 10^{-3} && \text{over land.} \end{aligned} \qquad \ldots (7.2)$$

H is the topography height in metres. These values have been chosen partly by consideration of published values for different surfaces, and partly from experience of model behaviour. The topographic dependence of C_D over land is intended to avoid sharp discontinuities at coasts, and also to make some allowance for form drag over mountains.

(*b*) The friction layer is assumed to be confined to the lowermost 100 mb of the model. A quadratic profile is assumed for τ in that layer with $\tau = 0$ and $\tau_p = 0$ at 900 mb. Thus

$$(\tau_p)_{10} = 2\tau_{10}/\Delta p, \qquad \ldots (7.3)$$

and $\tau_p = 0$ at all other co-ordinate surfaces.

Equations (7.1) and (7.3) are used to calculate tendencies $\dot{u}^*_F$, $\dot{v}^*_F$ (due to surface friction) of the 1000-mb velocity components u^*_{10}, $\dot{v}^*_{10}$ (see section 3.7).

$$\begin{aligned} \dot{u}^*_F &= -\frac{2g\rho_{10} C_D}{\Delta p} \left[\mu \left\{(u^*)^2 + (\overline{v^*}^{xy})^2\right\}\right]^{\frac{1}{2}} u^* \\ \dot{v}^*_F &= -\frac{2g\rho_{10} C_D}{\Delta p} \left[\mu \left\{(\overline{u^*}^{xy})^2 + (v^*)^2\right\}\right]^{\frac{1}{2}} v^* . \end{aligned} \qquad \ldots (7.4)$$

7.2. *Surface exchanges of sensible and latent heat: basic relationships*

The fluxes of sensible heat and water vapour into the model atmosphere across the 1000-mb surface are expressed as follows by conventional bulk aerodynamic formulae.

†Hayes (1975) has described an alternative formulation in which frictional effects are applied near the topography height and wind components at lower levels are set to zero. This formulation was used in the rectangle from January 1975 onwards.

$$F_H = \rho_{10} C_E |\mathbf{V}_{10}| c_p (T_o - T_a)$$
$$F_W = \rho_{10} C_E |\mathbf{V}_{10}| (r_o - r_a). \qquad \ldots (7.5)$$

The suffix 'o' denotes surface values whilst the suffix 'a' denotes values at a level in the atmosphere close to the surface (say the 10-m level). T_a and r_a must be estimated from parameters available in the 10-level model. As in the frictional formulation, the ICAO standard-atmosphere 1000-mb value is used for ρ_{10}.

The following procedure has been adopted for the calculation of T_a.

$$T_a = \begin{cases} T_{9.5} + \tfrac{1}{2} h'_{9.5} \gamma_d & \text{if } T_a < T_o \\ 0.1\,(T_{9.5} + \tfrac{1}{2} h'_{9.5} \gamma_9) + 0.9\, T_o & \text{if } T_a > T_o \\ T_o & \text{otherwise.} \end{cases}$$

Here $T_{9.5}$ is the temperature derived from $h'_{9.5}$ using the relationship

$$T_{9.5} = B_{9.5} h'_{9.5} = \frac{g h'_{9.5}}{R \log_e (10/9)}$$

γ_d is the dry adiabatic lapse rate, and γ_9 is the temperature lapse rate at 900 mb in the model atmosphere defined by $h'_{9.5}$ and $h'_{8.5}$.

The calculation of T_a set out above is based on the following assumptions.

(a) The layer from 950 mb to the 10-m level is characterized by a dry adiabatic lapse rate if the air is being heated from below.

(b) If the air is being cooled from below the shape of the temperature profile is such that the temperature difference between the surface and the 10-m level is one-tenth of that indicated by extrapolation from temperatures at 850 mb and 950 mb.

(c) If neither of these two models leads to a self-consistent result, it is assumed that there is no heat exchange and $T_a = T_o$.

The calculation of r_a is as follows.

$$r_a = X_a r_s (T_a, p_{10})$$

where $$X_a = \begin{cases} X_{9.5} & \text{if } T_a < T_o \\ 0.1 X_{9.5} + 0.9 X_0 & \text{if } T_a \geqslant T_o. \end{cases}$$

The relative humidity at 950 mb is assumed to be representative of air at the 10-m level in unstable conditions. This model was adopted when experience showed that the assumption of uniform humidity mixing ratio in the boundary layer led to unrealistically moist predictions in the lowest 100-mb layer. In stable conditions a relative humidity profile is assumed in which one-tenth of the change from surface to 950 mb takes place in the lowest 10 metres.

Consistent with the structure of the 10-level model (see section 1.3) the aerodynamic relationships are evaluated as if the earth's surface and the 1000-mb surface were coincident.

The balance at the earth's surface is described by the equation

$$F_H + LF_W = R_N - F_G,$$

which it is convenient to write as

$$F_H + LF_W = (1 - \chi)R_N. \quad \ldots (7.6)$$

7.3. *The surface energy fluxes over the sea*

The sea surface temperature T_o is regarded as constant during a forecast, and the humidity mixing ratio at the sea surface is taken to be the saturation value, $r_o = r_s\,(T_o, p_{10})$. Thus over the sea F_H and F_W may be calculated directly from equations (7.5). The exchange coefficient

$$C_E = \left(1 + \frac{T_o - T_a}{10}\right) \times 10^{-3}$$

is used, and is designed to take some account of the observed variation of exchange coefficients with stability.

7.4. *The surface energy fluxes over land*

Over land the direct application of equations (7.5) is prevented by the fluctuations of T_o in response to the net radiation flux R_N. A combined aerodynamic/energy-balance approach analagous to that suggested by Penman (1948) has been used, and the calculation of F_H and F_W falls into three parts as described below.

(a) *The net radiation flux*

Stanhill *et alii* (1966) have suggested the following approximate relationship between the net vertical radiation flux at the surface, R_N, and the vertical flux of incoming solar radiation, $SF'\sin\psi$, for cloudless skies.

$$R_N = (1 - \alpha)\,SF'\sin\psi - L'_0, \quad \ldots (7.7)$$

where α is the surface albedo and L'_0 is a constant of regression with the suggested value 0.13 cal cm^{-2} min^{-1} (90.7 J m^{-2}s^{-1}). The following transmission function for clear skies, F', determined empirically by Lumb (1964) has been used.

$$F' = 0.6 + 0.2\sin\psi. \quad \ldots (7.8)$$

The following formula has been used to calculate $\sin\psi$,

$$\sin\psi = \sin\delta\,\sin\phi - \cos\delta\,\cos\phi\,\cos\left(\frac{\pi t}{12} + \lambda\right), \quad \ldots (7.9)$$

where t is GMT in hours and δ, the solar declination, has been assigned the monthly values given in Table V. When $\sin\psi$ thus calculated is negative, the sun is below the horizon and equation (7.7) is reduced to $R_N = -L_0$.

It remains to account for the effects of cloud on the net radiation flux. Empirical relationships, based on the work of Ricketts (1973), have been used to derive fractional

areas of high, medium, and low-cloud cover from the relative humidities of the moistest 100-mb layers in the 300–500-mb, 500–800-mb, and 800–1000-mb groups respectively, These relationships are illustrated by Figure 5.

TABLE V. *Monthly values of* sin δ *and* cos δ *used in equation* (7.9)

Month	sin δ	cos δ
Jan.	−0.3597	0.9331
Feb.	−0.2291	0.9734
Mar.	−0.0387	0.9992
Apr.	0.1617	0.9868
May	0.3200	0.9474
June	0.3949	0.9187
July	0.3668	0.9303
Aug.	0.2431	0.9700
Sept.	0.0560	0.9984
Oct.	−0.1457	0.9893
Nov.	−0.3094	0.9509
Dec.	−0.3924	0.9198

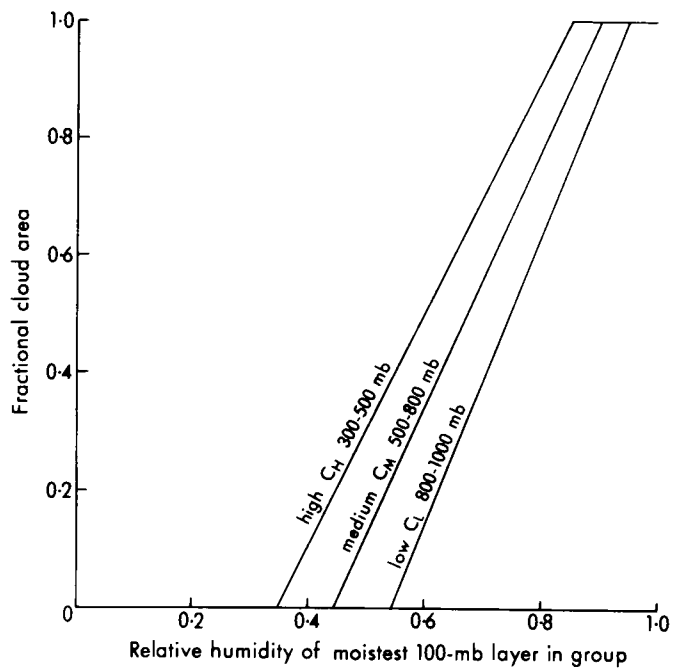

FIGURE 5. The relationships used to determine fractional cloud areas

The effects of cloud on net radiation have been represented by replacing the clear-sky parameters F' and L'_o in equation (7.7) by F and L_o, where

$$F = F' (1 - 0.4C_H) (1 - 0.7C_M) (1 - 0.7C_L) \quad \ldots (7.10)$$

$$L_o = L'_o (1 - 0.1C_H - 0.3C_M - 0.6C_L) \quad \ldots (7.11)$$

where C_H, C_M, C_L are the fractional cloud areas given by Figure 5. The coefficients of equation (7.10) have been chosen with reference to the work of Lumb (1964). The form of equation (7.11) is that discussed by Kondrat'yev (1965),

(b) *The heat flux into the ground*

During the daytime F_G is a relatively small component of the surface energy balance, and so a fairly crude specification of χ is adequate for the present purposes. The observations reported by Brooks and Goddard (1966) have been used to choose day-time and night-time values of χ for snow-free surfaces. The poor conductivity of snow is represented by setting $F_G = 0$.

$$\chi = \begin{cases} 0.0 \text{ for snow-covered surfaces;} \\ 0.1 \text{ for snow-free surfaces with } R_N > 0; \\ 0.5 \text{ for snow-free surfaces with } R_N \leqslant 0. \end{cases}$$

(c) *Partitioning the available energy into sensible and latent heat*

Using the procedures described above it is possible to calculate the energy flux $R_N - F_G$ available at the land surface for transfer into the atmosphere; it remains to partition this energy into sensible and latent forms.

During the night the latent heat flux into the atmosphere over vegetation is close to zero owing to stomatal closing. Also the contribution of dew formation has been neglected. Accordingly for $R_N \leqslant 0$ the surface flux relationships reduce to $F_W = 0$, $F_H = 0.5R_N$.

For $R_N > 0$ a method analogous to that of Penman is used as follows. The humidity mixing ratio at the surface is approximated by

$$r_o = X_o\, r_a\, (T_o, p_{10}) = X_o \left[r_s\, (T_a, p_{10}) + (T_o - T_a) \left(\frac{\partial r_s}{\partial T} \right)_p \right].$$

Using this relationship together with equation (7.5), the surface temperature T_o may be eliminated and the following equation obtained

$$LF_W = LF_W{}^* + X_o q F_H, \quad \ldots (7.12)$$

where $F_W{}^* = \rho_{10} C_E |V_{10}| (X_o - X_a)\, r_s\, (T_a, p_{10})$ and $q = \dfrac{L}{c_p} \left(\dfrac{\partial r_s}{\partial T} \right)_p$.

$F_W{}^*$ is constrained to be $\geqslant 0$ to prevent unrealistic effects when X_o is small; q may be evaluated by using the Clausius-Clapeyron equation as follows.

$$q = \frac{L}{c_p} \left(\frac{\partial r_s}{\partial T} \right)_p = \frac{\epsilon L^2 r_s\, (T_a, p_{10})}{c_p\, R T_a{}^2}.$$

Equations (7.6) and (7.12) may be solved simultaneously to give

$$F_H = \frac{(1 - \chi)R_N - LF_W^*}{1 + X_o q}, \quad LF_W = \frac{LF_W^* + X_o q\,(1 - \chi)R_N}{1 + X_o q} \qquad \ldots (7.13)$$

Conditions at the surface are represented by the surface relative humidity X_o which must be specified along with the surface albedo α. In the calculation of F_W^* the exchange coefficient

$$C_E = 1.0 \times 10^{-3}$$

is used. The required values of T_a and r_a are calculated as far as possible according to the assumptions set out in section 7.2. An unstable solution is first sought, using $T_a = T_{9.5} + \frac{1}{2}h'_{9.5}\,\gamma_d$ and $X_a = X_{9.5}$. This is the desired solution if the resulting F_H is positive, but if not, a stable solution must be examined. For this $T_a = T_{9.5} + \frac{1}{2}h'_{9.5}\gamma_9$ and $(X_o - X_a) = 0.1\,(X_o - X_{9.5})$ are used in the expression for F_W^*. If neither the unstable nor the stable assumption leads to self-consistent results, a neutral solution is chosen with $F_H = 0$, $LF_W = (1 - \chi)R_N$.

7.5. *The surface energy fluxes over sea-ice*

Sea-ice surfaces are treated as land surfaces except that the heat flux through the ice is expressed as

$$F_G = c_i\,(T_o - T_s), \qquad \ldots (7.14)$$

where $c_i = c/\Delta Z$, c is the thermal conductivity of sea-ice, ΔZ is a representative ice thickness, and T_s is the temperature at the ice/water interface. This formula is discussed by Vowinckel (1964). The values $c = 2$ J m m^{-2} s^{-1} K^{-1}, $\Delta Z = 150$ cm, $T_s = 271$ K have been used.

Equation (7.14) may be incorporated into the Penman algebra of the previous section and the following modified expressions for F_H and F_W at sea-ice surfaces result.

$$F_H = \frac{R_N - LF_W^* + c_i\,(T_s - T_a)}{1 + X_o q + d_i}$$

$$LF_W = \frac{X_o q\,(R_N + c_i\,(T_s - T_a)) + (1 + d_i)\,LF_W^*}{1 + X_o q + d_i} \qquad \ldots (7.15)$$

where $d_i = c_i/(\rho_{10} C_E |V_{10}| c_p)$.

If $|V_{10}| = 0$ the singularity is avoided by setting $F_H = F_W = 0$. The procedure for choosing an appropriate unstable, stable, or neutral solution is carried out as for land surfaces. The same exchange coefficient $C_E = 10^{-3}$ is used and the extrapolated temperature $T_a = T_{9.5} + \frac{1}{2}h'_{9.5}\,\gamma_9$ is used in the stable and neutral cases. The neutral solution is $F_H = 0$, $LF_W = R_N + c_i\,(T_s - T_a)$.

7.6. *Further measures at snow and ice surfaces*

(a) At snow and ice surfaces F_W is allowed to be non-zero (but not negative) even if $R_N < 0$ (see section 7.4).

(b) If $T_{9.5} > 273$ K the snow or ice surface is assumed to be melting. Equations (7.5) are applied directly with $T_o = 273$ K and $r_o = r_s(T_o, p_{10}) = 3.8$ g/kg.

7.7. *Surface parameters*

(a) Monthly mean sea surface temperatures and monthly mean distributions of sea-ice are used. Over land a climatic classification due to Trewartha (1968) is used, augmented in the fine-mesh version by mean maximum annual precipitation deficit data given by Mohrmann and Kessler (1959). The climatic classification is given in Table VI. Also over land a climatological snow-cover index is used to provide a classification according to snow-cover season. The snow-cover maps of Dickson and Posey (1967) have been used to define the period during which there is a greater than 50 per cent probability of snow cover one inch (*c.* 25 mm) or more in depth. Certain snow-covered areas in October and May were neglected for simplicity and Iceland (which does not appear on the maps) has been assigned a November–April snow-cover season. The snow-cover index is defined in Table VII. Climatic type 9 and snow-cover type 4 are coincident.

TABLE VI. *The climatic classifications*

Climatic type	Trewartha's groups	Octagon name	Rectangle classification
1	arid	arid	arid
2	semi-arid	semi-arid	semi-arid
3	tropical wet and dry	tropical wet and dry	subtropical/temperate, max. precip. deficit > 400 mm
4	subtropical dry summer	subtropical dry summer	subtropical/temperate, max. precip. deficit > 200 mm
5	temperate continental	temperate continental	subtropical/temperate, max. precip. deficit > 50 mm
6	tropical wet subtropical humid temperate oceanic highland	permanently moist	subtropical/temperate, max. precip. deficit < 50 mm
7	boreal	boreal	boreal
8	tundra	tundra	tundra
9	ice-cap	ice-cap	ice-cap
10	–	sea-ice	sea-ice

TABLE VII. *The climatic snow-cover index*

Snow-cover index	0	1	2	3	4
Snow-cover season	no snow cover	Jan. & Feb.	Dec.–Mar.	Nov.–Apr.	permanent

(b) *Albedo*

Values of the surface albedo α have been selected for each climatic type with and without snow and are presented in Table VIII. The values for types 1–8 were selected using the work of Kung *et alii* (1964), that for type 9 using the work of Diamond and Gerdel (1958), and that for type 10 using the work of Donn and Shaw (1966).

TABLE VIII. *Surface albedo*

Climatic type	α without snow	α with snow
1	0.25	0.40
2	0.20	0.40
3–6	0.15	0.40
7	0.15	0.50
8	0.20	0.80
9	–	0.80
10	0.60	0.60

(c) *Surface relative humidity*

$X_0 = 0.8$ is taken to be representative of vegetated surfaces with no significant soil moisture deficit. Szeicz and Long (1969) have indicated that surface resistance to evaporation is not much increased until soil moisture deficits exceed 40 mm for grass and 120 mm for trees. Hence $X_0 = 0.8$ is used throughout the year for climatic types 6, 7, and 8. At snow and ice surfaces air is saturated with respect to ice, and $X_0 = 1.0$ is used. For remaining categories values of X_0 have been guessed. $X_0 = 0.0$ and $X_0 = 0.2$ have been assigned to arid and semi-arid areas (types 1 and 2) respectively. The remaining types 3, 4, and 5 have been assigned seasonal variations separately for octagon and for rectangle. In the case of the rectangle the seasons of reduced X_0 were selected using Mohrmann and Kessler (1959). The month-by-month seasonal variations are given in Table IX.

TABLE IX. *Seasonal variation of surface relative humidity*

	Climatic type	Jan.	Feb.	Mar.	Apr.	May	June	July	Aug.	Sept.	Oct.	Nov.	Dec.
Octagon	3	0.5	0.4	0.3	0.2	0.2	0.5	0.8	0.8	0.8	0.9	0.7	0.6
	4	0.8	0.8	0.8	0.8	0.8	0.6	0.4	0.2	0.5	0.8	0.8	0.8
	5	0.8	0.8	0.8	0.8	0.8	0.7	0.5	0.4	0.6	0.8	0.8	0.8
Rectangle	3	0.8	0.8	0.7	0.6	0.5	0.4	0.3	0.2	0.4	0.6	0.8	0.8
	4	0.8	0.8	0.8	0.7	0.6	0.6	0.5	0.4	0.6	0.8	0.8	0.8
	5	0.8	0.8	0.8	0.8	0.7	0.7	0.6	0.6	0.7	0.8	0.8	0.8

7.8. *The effect of the surface fluxes on the model atmosphere*

The preceding sections set out the methods by which F_H and F_W, the fluxes of sensible heat and water vapour into the model atmosphere across the 1000-mb surface, are calculated. For reasons of computational economy F_H and F_W are recalculated at intervals of one hour during the integrations. Their effect on the model atmosphere, however, is calculated during each time-step of the integration.

The fluxes F_H and F_W are converted into increments $\delta h'$ and δr which correspond to the changes in the thickness $h'_{9.5}$ and humidity mixing ratio $r_{9.5}$ of the lowest 100-mb layer which would take place during a time-step δt if all the energy from the surface were retained in that layer. It may be shown that

$$\delta h' = \frac{R}{c_p} \frac{\log_e (\frac{10}{9})}{\Delta_p} \delta t F_H, \quad \delta r = \frac{g \delta t F_W}{\Delta_p} .$$

If the static stability in the model atmosphere permits, the effects of the surface fluxes may be distributed through two or more 100-mb layers by the convective-adjustment scheme described in the following section.

7.9. *Computational details*

The fluxes F_H and F_W and the corresponding increments $\delta h'$, δr, are calculated at the basic mesh points and all the required variables are available at these points except the 1000-mb wind speed $|\mathbf{v}_{10}|$. This speed is calculated as

$$|\mathbf{v}_{10}| = \left[\mu \left\{ (\overline{u}^{*y})^2 + (\overline{v}^{*x})^2 \right\} \right]^{\frac{1}{2}}$$

for the Lax-Wendroff grid and as

$$|\mathbf{v}_{10}| = \left[\mu \left\{ (\overline{u}^{*x})^2 + (\overline{v}^{*y})^2 \right\} \right]^{\frac{1}{2}}$$

for the semi-implicit grid.

The fields of $\delta h'$ and δr are smoothed using a nine-point operator before being added to $h'_{9.5}$ and $r_{9.5}$. In the absence of such smoothing unrealistic cold spots develop near coasts with an offshore wind in winter.

8. CONVECTIVE ADJUSTMENTS

8.1. *Introduction*

The representation of the effects of sub-grid-scale convective motions in numerical models of the atmosphere has several aspects. The convective adjustments scheme described in this section is designed primarily to prevent the growth of meteorologically unrealistic scales of convective motion (so-called grid-scale convection) in the model atmosphere. In addition it provides a realistic treatment of the redistribution of heat from the surface through the lower atmosphere by shallow cumulus. The scheme is inadequate in respect of deep cumulus convection and the associated convective rainfall, whilst even in the case of shallow convection the humidity transports are poorly represented.†

†Hayes (1975) has described a deep cumulus parametrization scheme designed to remedy these deficiencies. The scheme was used in the rectangle from June 1975 onwards.

8.2. *Basic assumptions of the convective-adjustment scheme*

The scheme rests on three basic assumptions which may be stated as follows.

(a) It is assumed that vertical heat transport effected by sub-grid-scale convection is sufficient to maintain a neutral lapse rate of grid-scale temperature wherever this would otherwise be exceeded. The neutral value γ_c of the temperature lapse rate $\gamma = -\partial T/\partial Z$ is taken to be

$$\gamma_c = \begin{cases} \gamma_d & 0 \leqslant X \leqslant X_c \\ \gamma_d \left(\dfrac{1 \quad X}{1 - X_c}\right) + \gamma_s \left(\dfrac{X \quad X_c}{1 - X_c}\right) & X_c \leqslant X \leqslant 1 \end{cases} \qquad \ldots (8.1)$$

Notice that γ_c is a continuous function of the grid-scale relative humidity X. If X is less than some threshold value X_c, γ_c is equal to the dry adiabatic lapse rate γ_d. If X is greater than X_c, γ_c increases linearly with X and is equal to the saturated adiabatic lapse rate γ_s when the model atmosphere is fully saturated on the grid scale. (At present $X_c = 0$ is used.)

(b) It is assumed that the vertical transport of water vapour by the convective motions are such that the grid-scale relative humidity remains unchanged. (On occasion this could lead to an increase in total water content; this possibility is dealt with in the following section.) Water vapour in excess of that required to conserve relative humidity is assumed to condense, and if the liquid water thus formed reaches the surface it is regarded as convective rainfall.

(c) It is assumed that the vertically integrated sum of potential, internal and latent energies, that is

$$\int (c_p T + Lr) \mathrm{d}p$$

is conserved by the convective motions.

8.3. *Details of the convective adjustment scheme*

It is convenient to define a function $b(X)$ such that $\gamma_c = b\gamma_d$. Equation (8.1) may be expressed in terms of potential temperature as follows

$$\frac{\partial \theta}{\partial p} = -\frac{R}{c_p}\frac{\theta}{p}(1 - b), \qquad \ldots (8.2)$$

in order that the convective adjustments may be carried out in a manner consistent with the model's thermodynamic equation (see sections 3 and 4). Since $b(X)$ may be conveniently calculated at the mid points of the 100-mb layers, the following finite difference analogue of equation (8.2) is used at level k.

$$\frac{\theta_{k+\frac{1}{2}} - \theta_{k-\frac{1}{2}}}{\Delta p} = -\frac{R}{c_p}\left[\frac{1}{2}\left\{\frac{\theta_{k+\frac{1}{2}}(1 - b_{k+\frac{1}{2}})}{p_{k+\frac{1}{2}}} + \frac{\theta_{k-\frac{1}{2}}(1 - b_{k-\frac{1}{2}})}{p_{k-\frac{1}{2}}}\right\}\right].$$

Notice that, since the model atmosphere is dry above 300 mb, $b_{1.5} = b_{2.5} = 1$. By algebraic manipulation the following expression is obtained

$$h'_{k+½} = C_k \, h'_{k-½} \, ,$$

where, using $p_{k+½} = (k + ½)\,\Delta p$, $c_p = 3.5R$, $\theta_{k+½} = A_{k+½} \, h'_{k+½}$, it may be shown that

$$C_k = \frac{(7\,(k - ½) - 1 + b_{k-½})\,(k + ½)\,A_{k-½}}{(7\,(k + ½) + 1 - b_{k+½})\,(k - ½)\,A_{k+½}} \, .$$

After each complete time-step of integration the eight levels from 200 mb to 900 mb, corresponding to $k = 2, 3, \ldots, 9$, are tested for instability at each grid point. Level k is regarded as unstable if

$$h_{k+½} > C_k \, h'_{k-½} \, .$$

The eight levels are tested in this way beginning at 200 mb and working downwards. If k_1 is the first level found to be unstable and if $k_2 = k_1 + n$ is the next stable level ($k_2 = 10$ if no further stable level is found), the $n + 1$ thicknesses and $n + 1$ mixing ratios of layers $k_1 - ½, k_1 + ½, \ldots . k_2 - ½$ are adjusted as follows. Naturally, if no levels are found to be unstable, no further action is taken.

The values of variables after convective adjustment are indicated by stars. The requirement that levels $k_1, k_1 + 1, \ldots k_2 - 1$ be neutrally stable after adjustment gives the following n equations in the $n + 1$ adjusted thicknesses.

$$h'^*_{k+½} = C^*_k \, h'^*_{k-½} \, , \qquad \ldots (8.3)$$

where $k = k_1, k_1 + 1, k_2 - 1$.

Since it is assumed that relative humidity is unchanged by the convection, $C^*_k = C_k$.

The same assumption gives $n + 1$ equations in the $n + 1$ adjusted humidity mixing ratios.

$$r^*_{k-½} = X_{k-½} \, r_s{}^*_{k-½} \, , \qquad \ldots (8.4)$$

where $k = k_1, k_{1+1}, \ldots k_2$. Note that if $k \leqslant 3$, $X_{k-½} = 0$.

Using a linear approximation to the Clausius-Clapeyron equation, $r_s{}^*_{k-½}$ may be related to $T^*_{k-½}$ as follows (as usual, $T^*_{k-½} = B_{k-½} \, h'^*_{k-½}$).

$$r_s{}^*_{k-½} = r_{sk-½} + \frac{\epsilon L r_{sk-½}}{RT^2_{k-½}} \, (T^*_{k-½} - T_{k-½}) . \qquad \ldots (8.5)$$

The set of simultaneous equations may now be completed by a finite-difference analogue of assumption (c) above (page 34), namely

$$\sum_{k=k_1}^{k_2} \left[c_p \, (T^*_{k-½} - T_{k-½}) + L \, (r^*_{k-½} - r_{k-½}) = 0 \right] . \qquad \ldots (8.6)$$

Substituting (8.4) and (8.5) successively into (8.6) the following equation is obtained

$$\sum_{k=k_1}^{k_2} \left[\left(c_p + \frac{\epsilon L r_{k-\frac{1}{2}}}{RT^2{}_{k-\frac{1}{2}}} \right) \left(T^*{}_{k-\frac{1}{2}} - T_{k-\frac{1}{2}} \right) \right] = 0. \qquad \ldots (8.7)$$

Again, if $k \leqslant 3$, $r_{k-\frac{1}{2}} = 0$.

Using $T_{k-\frac{1}{2}} = B_{k-\frac{1}{2}} h'_{k-\frac{1}{2}}$, and substituting equation (8.3), equation (8.7) may be reduced to an equation for the single unknown $h'^*{}_{k_1-\frac{1}{2}}$. Equation (8.3) is now used to obtain the other adjusted thicknesses, new values of saturation mixing ratio are calculated from the adjusted thicknesses, and the adjusted values of humidity mixing ratio are obtained using equation (8.4), thus completing the solution.

The mixing ratio of liquid water falling through level k_2 as a result of the convective adjustment is given by

$$M_{k_2} = \sum_{k=k_1}^{k_2} (r_{k-\frac{1}{2}} - r^*_{k-\frac{1}{2}}).$$

If M_{k_2} computed in this way is negative, assumption (b) above (page 34) is inapplicable and a second solution of the convective adjustment is calculated. In this case there is no latent heat release, $M_{k_2} = 0$, and the adjusted thicknesses are obtained by solving equation (8.3) together with

$$\sum_{k=k_1}^{k_2} (T^*_{k-\frac{1}{2}} - T_{k-\frac{1}{2}}) = 0.$$

In this second solution the relative humidity of the uppermost adjusted layer is reduced so that the total water content of the adjusted layers is conserved.

A convective adjustment made in this way to layers $k_1-\frac{1}{2}, k_1+\frac{1}{2}, \ldots k_2-\frac{1}{2}$ may possibly create instability at the (previously stable) levels k_1-1 or k_2. The stability of these levels is therefore tested after adjustment and if, for example, level k_2 is now found to be unstable the adjustment is repeated, this time involving layers $k_1-\frac{1}{2}, k_1+\frac{1}{2}, \ldots k_2-\frac{1}{2}, k_2+\frac{1}{2}$. By an iterative process it is ensured after the convective adjustment is completed that the entire column of the model atmosphere is free from instability according to the criterion described above. Convective adjustment may take place in two, or conceivably more, separate sets of contiguous layers in a given vertical column.

8.4 *Additional features*

(a) *Arid regions.* In arid regions the convective-adjustment scheme could produce unrealistic convective rainfall unless special precautions were taken. Therefore if $X_{k_2-\frac{1}{2}} < 0.5$, the second solution of the convective adjustment, in which there is no possibility of convective rainfall, is always calculated. (A similar strategy has been adopted in the boundary zone of the model atmosphere in the case of semi-implicit integrations.)

(b) *Ice phase.* No account of the ice phase is taken in the convective-adjustment scheme, except that if $T_{k2-\frac{1}{2}} < 273$ K the latent heat sublimation is used in place of the latent heat of vaporization in equation (8.7). The purpose of this measure is to avoid an inconsistent heat sink in the modelling of the melting layer (see section 6).

(c) *Evaporation of convective rainfall.* The convective rainfall represented by M_{k_2} is subject to evaporation as it falls towards the surface (see section 6). For this purpose it is assumed that the convective rainfall is falling in only 5 per cent of the grid square and consequently the convective rainfall rate (e.g. P_{k_2}) is multiplied by 20 before the effects of evaporation are calculated, whilst the resulting rainfall rate (e.g. P_{k_2+1}) is subsequently divided by the same factor.

8.5. *The redistribution of surface fluxes*

The following sequence of operations is used to represent the distribution of sensible heat and water vapour from the surface through the lower layers of the model atmosphere.

(a) After each time-step of integration the thickness increment $\delta h'$ due to surface fluxes (see section 7.8) is added to $h'_{9.5}$ (see section 4 for special procedures in semi-implicit integrations).

(b) The humidity increment δr due to surface fluxes is uniformly distributed among the set of 100-mb layers adjacent to the surface which were involved in a convective adjustment at the end of the previous time-step. If there was no convective adjustment adjacent to the surface δr is added to $r_{9.5}$. When the humidity of any layer is enhanced by the surface flux, a check is made to ensure that supersaturation does not occur. If necessary, water vapour is discarded to prevent supersaturation, implying a corresponding reduction in the surface flux of water vapour (F_W).

(c) Finally the convective-adjustment scheme is operated as described above. If the static stability permits this will distribute the effects of F_H (the surface flux of sensible heat) through two or more 100-mb layers.

TABLE X. *The constants $A_{k+½}$ and $B_{k+½}$ used to convert the thickness of a 100-mb layer ($h'_{k+½}$) into potential temperature and temperature respectively*

Pressure *mb*	k	$A_{k+½}$	$B_{k+½}$
150	1	0.0847259	0.0492559
250	2	0.1251998	0.0842035
350	3	0.1602155	0.1186782
450	4	0.1923245	0.1530028
550	5	0.2222779	0.1872603
650	6	0.2504960	0.2214819
750	7	0.2776707	0.2556821
850	8	0.3034922	0.2898684
950	9	0.3289063	0.3240453

BIBLIOGRAPHY

BENWELL, G. R. R., GADD, A. J., KEERS, J. F., TIMPSON, MARGARET S. and WHITE, P. W. 1971 The Bushby-Timpson 10-level model on a fine mesh. *Scient Pap, Met Off*, No. 32.

BEST, A. C. 1952 The evaporation of raindrops. *Q J R Met Soc*, 78, pp. 200–225.

BROOKS, F. A. and GODDARD, W. B. 1966 Investigation of energy, momentum, and mass transfers near the ground. Davis, University of California, Dep. Agric. Engng and Dep. Wat. Sci. Engng (Grant DA–AMC–28–043–65–512, Final Report), pp. 5–24.

BURRIDGE, D. M. 1975 A split semi-implicit reformulation of the Bushby-Timpson 10-level model. *Q J R Met Soc*, **101**, pp. 777–792.

BUSHBY, F. H. and TIMPSON, MARGARET S. 1967 A 10-level atmospheric model and frontal rain. *Q J R Met Soc*, **93**, pp. 1–17.

DIAMOND, M. and GERDEL, R. W. 1958 Radiation measurements on the Greenland Ice Cap. Int. Ass. Sci. Hydrol., Gentbrugge, Publ No. 46.

DICKSON, R. R. and POSEY, J. 1967 Maps of snow cover probability for the Northern Hemisphere. *Mon Weath Rev*, **95**, pp. 347–353.

DONN, W. L. and SHAW, D. M. 1966 The heat budgets of an ice-free and an ice-covered Arctic Ocean. *J Geophys Res*, 71, pp. 1087–1093.

FARR, M. A. L. and LEWIS, R. P. W. 1971 Criterion for computational stability in the 10-level model. *Scient Pap, Met Off*, No. 32, Appendix II.

GADD, A. J. 1973 On the calculation of static stability in the 10-level model. (Unpublished, copy available in the Meteorological Office Library, Bracknell.)

1974 Fourth-order advection schemes for the 10-level model. (Unpublished, copy available in the Meteorological Office Library, Bracknell.)

HAYES, F. R.	1975a	A parametrization of deep precipitating cumulus for use in the Meteorological Office operational 10-level model. (Unpublished, copy available in the Meteorological Office Library, Bracknell.)
	1975b	A representation of topography and the surface boundary layer in the Meteorological Office 10-level model. (Unpublished, copy available in the Meteorological Office Library, Bracknell.)
KONDRAT'YEV, K. Ya.	1965	Radiative heat exchange in the atmosphere. Oxford, Pergamon Press (translated from the Russian, first published in 1956).
KUNG, E. C., BRYSON, R. A. and LENSCHOW, D. H.	1964	Study of continental surface albedo on the basis of flight measurements and structure on the earth's surface cover over North America. *Mon Weath Rev*, **92**, pp. 543–564.
LUMB, F. E.	1964	The influence of cloud on hourly amounts of total solar radiation at the surface. *Q J R Met Soc*, **90**, pp. 43–56.
MARCHUK, G. I., VOROBIOV, V. P., DYMNIKOV, C. P. and KONTAREV, G. R.	1968	Short-term weather prediction by splitting of the complete hydrodynamic equations. *Proc. WMO/IUGG Symp. Num. Weath. Pred., Tokyo*, 1968. Japan Meteorological Agency, pp. II-1 –II-12.
MASON, B. J.	1957	The physics of clouds. London, Cambridge University Press.
MOHRMANN, J. C. J. and KESSLER, J.	1958	Water deficiencies in European Agriculture – a climatological survey. Wageningen, The Netherlands, International Institute for Land Reclamation and Improvement. Publication 5.
PENMAN, H. L.	1948	Natural evaporation from open water, bare soil and grass. *Proc R Soc*, **193**, A, pp. 120–145.
RICKETTS, J. N.	1973	An investigation into a relationship between upper-air relative humidity and cloud cover. *Met Mag*, **102**, pp. 146–156.
ROBERT, A. J., HENDERSON, J. and TURNBULL, C.	1972	An implicit time integration scheme for baroclinic models of the atmosphere. *Mon Weath Rev*, **100**, pp. 329–335.
SZEICZ, G. and LONG, I. F.	1969	Surface resistance of crop canopies. *Water Resources Research*, **5**, pp. 622–633.
STANHILL, G., HOFSTEDE, G. F. and KALMA, J. D.	1966	Radiation balance of natural and agricultural vegetation. *Q J R Met Soc*, **92**, pp. 128–140.
TREWARTHA, G. T.	1968	An introduction to climate. New York, McGraw-Hill.
VOWINCKEL, E.	1964	Heat flux through the polar ocean ice. Montreal, McGill University, Publications in Meteorology No. 70.
WEXLER, R.	1952	Precipitation growth in stratiform clouds. *Q J R Met Soc*, **78**, pp. 363–376.

Printed in England for Her Majesty's Stationery Office by Hobbs the Printers of Southampton
(309) Dd585869 K8 7/77

HER MAJESTY'S STATIONERY OFFICE

Government Bookshops

49 High Holborn, London WC1V 6HB
13a Castle Street, Edinburgh EH2 3AR
41 The Hayes, Cardiff CF1 1JW
Brazennose Street, Manchester M60 8AS
Southey House, Wine Street, Bristol BS1 2BQ
258 Broad Street, Birmingham B1 2HE
80 Chichester Street, Belfast BT1 4JY

Government publications are also available through booksellers

ISBN 0 11 400300 9